

Generating Topobathymetry Digital Elevation Model using Crowdsourced Bathymetry:
A case of the St. Lawrence River and Ottawa River in Quebec

Henish Goswami

A Thesis
in
The Department
of
Building, Civil and Environmental Engineering

Presented in Partial Fulfillment of the Requirements
for the Degree of Master of Applied Science (Civil Engineering) at
Concordia University
Montréal, Québec, Canada

October 2021

© Henish Goswami, 2021

CONCORDIA UNIVERSITY

School of Graduate Studies

This is to certify that the thesis prepared

By: **Henish Goswami**

Entitled: **Generating Topobathymetry Digital Elevation Model using Crowdsourced
Bathymetry: A case of the St. Lawrence River and Ottawa River in Quebec**

and submitted in partial fulfillment of the requirements for the degree of

Master of Applied Science (Civil Engineering)

complies with the regulations of the University and meets the accepted standards with respect to originality and quality.

Signed by the final Examining Committee:

Chair
Examiner

Dr. Catherine Mulligan

Examiner

Dr. Ciprian Alecsandru

Supervisor

Dr. Samuel Li

Approved by

Dr. Ashutosh Bagchi, Chair of Department

2021

Dr. Mourad Debbabi, Dean

Abstract

Generating Topobathymetry Digital Elevation Model using Crowdsourced Bathymetry:
A case of the St. Lawrence River and Ottawa River in Quebec

Henish Goswami

The accuracy of two- and three-dimensional hydraulic modelling of free surface flow depends significantly on a complete and accurate geometric description of the river channel and floodplains in the form of a continuous, seamless digital elevation model (DEM). With the advent of airborne Light Detection and Ranging (LiDAR) surveys, high-resolution topographic data is increasingly becoming available. However, bathymetric information for most rivers is not available in ready-to-use digital data formats, mainly because the primary data collection methods, i.e., hydrographic surveys, are costly and time-intensive. The existing methods for generating topobathymetry digital elevation model (TB-DEM) require access to raw data and ground measurements to some extent. This study proposes a simple superposition-based approach to generating a seamless elevation model using terrestrial and bathymetry information available from secondary data sources, including crowdsourcing. It comprises geographic information system (GIS) based interpolation and geoprocessing techniques. An integrated TB-DEM is generated for part of the St. Lawrence River and Ottawa River and the overbank areas on the upstream side of Montreal Island in Quebec. The output DEM is verified using internal and external validation criteria. The upland topography is unaffected by the superposition process, whereas the interpolated bathymetry shows significant positive linear associations with the reference elevation data. The vertical accuracy of bathymetry DEM with respect to Canadian Hydrographic Service Non-Navigational Bathymetric Data-10 (NONNA-10) reference data is 1.43 m in root-mean-squared error. The results of 1-m \times 1-m DEM from this study are useful for evaluations of fish habitat health, shoreline stability and drinking-water withdrawal-site selection, and for predictions of river floods, morphological changes, and changes of water quality. The methods are applicable to other sites for generating high-resolution DEMs.

Acknowledgements

Foremost, I would like to express my sincere gratitude to my supervisor Prof. S. Samuel Li, PhD, for the continuous support of my master's study and research, for his patience, motivation, enthusiasm, and immense knowledge. His guidance helped me all the time in my research and writing of this thesis.

Besides my supervisor, I would like to thank the rest of my thesis committee for their encouragement, insightful comments, and valuable feedback. I offer my sincere appreciation for the learning opportunities provided by my committee.

Last but not least, I would like to thank my parents, family members and friends for being with me at every moment and providing continuous morale-boosting and affection during my studies and beyond.

Table of Contents

List of Figures.....	vii
List of Tables.....	ix
List of Symbols	x
List of Abbreviations	xi
Chapter 1: Introduction.....	1
1.1 Background	1
1.2 Objectives.....	2
1.3 Thesis overview	3
Chapter 2: Literature Review	4
2.1 Importance of channel geometry in hydraulic modelling	4
2.2 What is bathymetry? How is it obtained?.....	5
2.2.1 Survey methods.....	5
2.2.2 Empirical methods	7
2.3 Need for Topobathymetry DEM.....	8
2.4 Crowdsourced bathymetry: A way forward	9
Chapter 3: Study Area and Materials.....	11
Chapter 4: Methodology	16
4.1 Superposition of topographic and bathymetric data.....	16
4.2 Generating river bathymetry DEM	20
4.3 Pre-processing LiDAR-derived topography DEM.....	24
4.4 Generating Topobathymetry DEM.....	29
Chapter 5: Results and Validation.....	33
5.1 Internal Validation	34
5.1.1 Georeferencing of bathymetry charts	34
5.1.2 Visual inspection of Bathymetry DEM	35

5.1.3 Deviation of filtered DEM from original DEM.....	37
5.2 External Validation	38
5.2.1 Comparing B-DEM and NONNA DEMs	38
5.2.2 Statistical validation of B-DEM using sample points	40
Chapter 6: Conclusion and Discussion	45
6.1 Key findings	45
6.2 Applications of Topobathymetry DEM	47
6.3 Examples from around the world	49
6.4 Future studies	50
Bibliography	51
Appendices.....	58

List of Figures

Figure-1: Flooding incidents reported in Canada between 1990-2020	1
Figure-2: Location of the study area on the upstream of Montreal Island	12
Figure-3: Process flow chart for generating Topobathymetry DEM.....	17
Figure-4: Schematic representation of a channel cross-section showing the superposition of LiDAR-derived topography onto SoNAR-derived bathymetry.....	18
Figure-5: Using image editing program to compile multiple image tiles and generating digital canvas of bathymetry chart	20
Figure-6: Georeferencing part-wise bathymetry chart with satellite imagery in ArcGIS.	22
Figure-7: Layers involved in the generation of Bathymetry DEM	23
Figure-8: Detecting artefacts of Triangulation-based errors using hillshade and slope raster.....	25
Figure-9: Detecting artefacts induced by the stitching of LiDAR survey grids using hillshade and slope raster	25
Figure-10: Detecting artefacts of unnaturally steep and shallow ground features using hillshade and slope raster	26
Figure-11: Terrain interpolation using point-elevations without buffer and with buffer (20m)	28
Figure-12: An illustration showing the superposition of Topography on Channel Bathymetry, giving the combined Topobathymetry	29
Figure-13: Seamless Topobathymetry DEM of the AOI at Montreal Island	31
Figure-14: Selected cross-sections (A-A) to (J-J) showing different terrain profiles.....	32
Figure-15: Incorrect depth value registered while digitizing contours from bathymetry chart; mutating the subsequent interpolated raster and vector features	36
Figure-16: Raster displaying the percentage by which the filtered T-DEM deviates from the raw LiDAR T-DEM.....	37
Figure-17: Comparing the coverage and data continuity of bathymetry rasters: B-DEM 1m, NONNA-10m and NONNA-100m	39

Figure-18: Comparison of sample point elevations from NONNA-10 and B-DEM..... 41

Figure-19: Histograms showing the distribution of sample points in B-DEM, NONNA-10
DEM and NONNA-100 DEM 42

Figure-20: Scatter plot of sample point elevations showing the relationship between (a)
B-DEM and NONNA-10; (b) B-DEM and NONNA-100..... 43

List of Tables

Table 1: Sources of topographic and bathymetric data used in this study..... 15

Table 2: Georeferencing links and errors..... 35

Table 3: Statistical summary of the bathymetry rasters..... 38

Table 4: Descriptive statistics of test sample points 40

Table 5: Correlation matrix 40

List of Symbols

Symbol	Definition
Z_i	elevation value of cell i of T-DEM in meter
h_i	elevation value of cell i from LiDAR DEM in meter
d_i	elevation value of cell i from bathymetry DEM in meter
x'	horizontal value in coordinate space in map units
y'	vertical value in coordinate space in map units
x	column-count of pixels in image space
y	row count of pixels in image space
A	width of the cell in map units
B	a rotation term
C	x' value of the center of upper-left cell
D	a rotation term
E	negative height of the cell in map units
F	y' value of the center of upper-left cell
ΔZ	percentage change in elevation of cell i
Z_f	elevation value of cell i of filtered T-DEM in meter
Z_r	elevation value of cell i of raw T-DEM in meter
$RMSE_Z$	the root-mean-squared error of elevation raster in meter
Z_{di}	B-DEM elevation value of point i in the sample dataset
Z_{ci}	NONNA DEM elevation value of point i in the sample dataset
n	number of sample points being checked

List of Abbreviations

Abbreviation	Definition
1D	One-dimensional
2D	Two-dimensional
ANUDEM	A program that calculates regular grid digital elevation models
AOI	Area of interest
AR6	Sixth Assessment Report
ASCII	American Standard Code for Information Interchange
ASTER	Advanced Spaceborne Thermal Emission and Reflection Radiometer
B-DEM	Bathymetry Digital Elevation Model
BIT	binary digit
CHS	Canadian Hydrographic Service
CoNED	Coastal National Elevation Database
CSRS	Canadian Spatial Reference System
DEM	Digital Elevation Model
DFO	Fisheries and Oceans Canada
DSM	Digital Surface Model
DTM	Digital Terrain Model
EAARL	Experimental Advanced Airborne Research Lidar
EAARL-B	second-generation Experimental Advanced Airborne Research Lidar
EPSG	European Petroleum Survey Group
ESRI	Environmental Systems Research Institute
GCP	ground control point
GIS	Geographic information system
GPS	Global Positioning System
IHO	International Hydrographic Organization

continued on next page

Abbreviation	Definition
IPCC	Intergovernmental Panel of Climate Change
LiDAR	Light Detection and Ranging
MFFP	Ministry des Forêts, de la Faune et des Parcs
MNRF	Ministry of Natural Resources and Forestry
MTM	Modified Transverse Mercator
NAD83	North American Datum of 1983
NOAA	National Oceanic and Atmospheric Administration
NONNA	Non-Navigational Bathymetric Data
NRCan	Natural Resources Canada
NSSDA	National Standard for Spatial Data Accuracy
NTS	National Topographic System
NTU	Nephelometric Turbidity Units
ORRPB	Ottawa River Regulation Planning Board
QGIS	A free and open-source geographic information system
RF	Random Forest
RMSE	Root-Mean-Square Error
SAGA	System for Automated Geoscientific Analyses
SoNAR	Sound Navigation and Ranging
SRTM	Shuttle Radar Topography Mission
SWOT	Surface Water and Ocean Topography
TB-DEM	Topobathymetry Digital Elevation Model
T-DEM	Topography Digital Elevation Model
TIFF	Tagged Image File Format
WSE	water surface elevation

Chapter 1:

Introduction

1.1 Background

Flood events across the globe are becoming more extreme and erratic due to climate change-related impacts (Berghuijs et al., 2017). Global warming is intensifying the water cycle and bringing more intense rainfall and associated flooding. The severe flooding in Western Europe due to very heavy rainfall during July 2021 was attributed to an estimated 500 year or rarer flood event at the Ahr river and resulted in at least 184 fatalities in Germany and 38 in Belgium (Kreienkamp et al., 2021). Similar extreme weather events were also observed during July and August 2021, with flooding occurring in China, Turkey, India, Afghanistan, Pakistan, the United States and New Zealand.

Flooding is the most common and costly natural hazard in Canada (Henstra & Thistlethwaite, 2018). As per the Canadian Disaster Database, 159 flooding incidents have been reported between 1990 and 2020 (Figure-1). Also, the Sixth Assessment Report (AR6)



Figure-1: Flooding incidents reported in Canada between 1990-2020
(Data Source: Canadian Disaster Database)

of the Intergovernmental Panel of Climate Change (IPCC) reported that the observed change in heavy precipitation since the 1950s has increased in the Central and Eastern North America region (IPCC, 2021). Though extreme precipitation does not necessarily result in maximum streamflow (Do et al., 2020), in some cases, it may become a driving factor that causes river flooding (Berghuijs et al., 2016).

Global hydrological models project a more significant fraction of land areas to be affected by an increase in river floods (Seneviratne et al., 2021). To better understand flooding, it is crucial to study the hydraulic behaviour of various rivers for the projected peak streamflows and identify flood inundation extents for probable scenarios. Hydraulic modelling of rivers depends on hydrologic input data and topographic data (Bhuyian et al., 2015). Most computer-aided hydraulic modelling programs include at least the following categories of workflows: (1) defining channel geometry, (2) setting up inflow-outflow conditions, and (3) performing hydraulic computations. Qualitatively, they are of equal importance and have a similar influence on the simulation results; however, each workflow category has advanced differently from a technological viewpoint. This study focuses on the aspects related to channel geometry and identify ways to improve the existing digital terrain modelling workflows.

1.2 Objectives

This study aims to generate a high-resolution, seamless Topobathymetry Digital Elevation Model (TB-DEM) using published LiDAR DEMs and crowdsourced bathymetry data, and proposing a superposition-based approach for integrating digital terrain information from disparate spatial data sources.

Following are the key objectives of the study:

- 1) To integrate channel bathymetry data with an existing DEM without affecting the details of upland topography.
- 2) To generate the highest possible resolution TB-DEM using publicly available data sources, including crowdsourcing.

- 3) To develop a simple approach for integrating topographic and bathymetric datasets without taking ground measurements or primary data collection surveys.

1.3 Thesis overview

The subsequent sections of the thesis are summarised as follows: Chapter-2 includes a comprehensive review of essential literature covering the subject matters relevant to this thesis. It explains the importance of river channel geometry in hydraulic modelling by highlighting the general modelling approaches, characteristics and types of input data, their acquisition methods, and recent developments in the area of crowdsourced bathymetry.

Chapter-3 describes the site of study and highlights key geographical features located in and around the study area. It also discusses the data sources used in this study, along with their attributes and sourcing methods.

Chapter-4 discusses the methodology by first explaining a novel and simple superposition-based approach for integrating topographic and bathymetric data. It proceeds to discuss the construction of a bathymetry DEM using crowdsourced data. This is followed by the detailed pre- and post-processing of the existing topography DEM and make it compatible with the final superpositioning process, which is discussed in the last section of the chapter.

Chapter-5 is dedicated to the presentation of the results of superpositioning bathymetry DEM with topography DEM. The resulting DEM is also subjected to internal and external validation techniques to test and further discuss the integrity and applicability of the combined topobathymetry DEM.

Chapter-6 mentions key findings drawn from the study, discusses applications of the output DEM, highlights similar examples from around the world, and provides suggestions for further enhancing topobathymetry DEM.

Chapter 2:

Literature Review

2.1 Importance of channel geometry in hydraulic modelling

The topography provides information about channel geometry and has a significant impact on hydrologic and hydraulic parameters (Vaze et al., 2010). The accuracy of flood mapping largely depends on the accuracy of model geometry (Flener et al., 2012). Errors in channel geometry data lead to additional uncertainties in the accuracy of hydraulic models (Bhuyian et al., 2015). Therefore, a complete and accurate geometric description of main channel bathymetry and floodplain topography is essential for obtaining reliable results from hydraulic numerical modelling (Laks et al., 2017; Lai et al., 2018; Bailly et al., 2010).

There are two generally and widely practised approaches for hydraulic modelling of rivers: One-dimensional (1D) and two-dimensional (2D). Flood modellers have increasingly used 2D hydraulic models to estimate inundation floodplains (Conner & Tonina, 2014). Studies have also demonstrated that a 2D hydraulic model results in a more realistic and accurate inundation extent than a 1D modelling approach (Cook & Merwade, 2009). Besides the hydraulic computation algorithms, 1D and 2D models differ in their physical description of the river channel and floodplain areas. In 1D models, the channel geometry is defined as cross-sectional measurements at a prescribed spatial interval. Whereas in 2D models, the geometry is described as a two-dimensional surface represented by a digital elevation model (DEM).

DEM is often generated based on remotely sensed data, including Spaceborne Photogrammetry-based DEMs and Airborne LiDAR-derived DEMs (LiDAR DEMs). The accuracy of publically available Advanced Spaceborne Thermal Emission and Reflection Radiometer (ASTER) DEM and Shuttle Radar Topography Mission (SRTM) DEM is

insufficient for hydraulic modelling (Walczak et al., 2016). Nevertheless, the global DEM data sources can be used as an input to 2D hydraulic modelling provided that the river bathymetry and floodplain topography are accurately reconstructed using ground observations (Tarekegn et al., 2010). Yamazaki et al. (2012) adjusted spaceborne SRTM3 DEM using a prescribed drainage network dataset and successfully removed the pits in DEM by minimizing post-processing requirements. However, the channel bed elevations are not represented in the adjusted DEM because the spaceborne DEMs did not primarily record the channel bathymetry.

On the other hand, Airborne LiDAR-derived DEMs are considered to be very accurate. Aerial laser scanning is a cost-effective way of developing a DEM with sufficient accuracy over a large area (Polidori & Hage, 2020). High spatial resolution and vertical accuracy of LiDAR measurements help resolve better overland drainage and improve the hydraulic modelling of stream-induced inundation (Gesch et al., 2016). However, most LiDAR topographic datasets do not include river bathymetry information (Flanagin et al., 2008; Cook & Merwade, 2009). A study has demonstrated that LiDAR DEM's description of the riverbed is inadequate, limiting their application for accurate hydraulic modelling (Bures et al., 2019).

2.2 What is bathymetry? How is it obtained?

Bathymetry describes the depths and shapes of underwater terrain, including the ocean, rivers, streams, and lakes (NOAA, 2021). It is critical to the accuracy of the hydraulic modelling of rivers (Dey, 2016). In addition, incorporating river bathymetry in topographic data improves the accuracy of flood inundation areas (Cook & Merwade, 2009). Bathymetry is obtained through hydrographic surveys and remote sensing methods.

2.2.1 Survey methods

Ship-based hydrographic surveys are still a significant source of bathymetric information (Gesch et al., 2016). It provides riverbed elevations in point features distributed across sparsely located cross-sections (Flanagin et al., 2008). A study suggested

that the cross-sectional bathymetry data should be collected at an interval of 1 times the average channel width in large rivers, preferably 0.5 times channel width if channel geometry is complex (Conner & Tonina, 2014). The suggested interval would result in many cross-sectional measurements to cover a large area of interest that comprises braided river reaches with fluvial lakes.

Remote sensing of bathymetry is limited only to clear and shallow river waters (Legleiter, 2021). It is divided into two categories: (1) Optical remote sensing and (2) active remote sensing. Optical remote sensing uses visible light and microwave radiation. It is based on the principle that the total amount of radiative energy reflected from a water column is a function of water depth. Optical sensing is appropriate for mapping bathymetry of entire river courses. It requires a model (either analytical or empirical) between radiance values on satellite imagery and the depths at sample locations. Depth modelling with optical remote sensing is affected by an obstructed view of the study area (possibly due to cloud cover, overhanging trees, shadows, or ice cover), turbid water, and water surface roughness due to ripples.

On the other hand, active remote sensing of bathymetry uses swath beam SoNAR and green-wavelength LiDAR sensors. These sensors transmit pulses of sound or light at short intervals over an area and receive the signal returned from the riverbed. The water column's depth is calculated from the time difference between the two pulses. Active remote sensing is usually costlier than optical remote sensing-based bathymetry (Flener et al., 2012).

The most significant limitation of aerial green LiDAR scanning is water turbidity (Bures et al., 2019). As a result, green LiDAR cannot differentiate between fine and coarse sediments (Costa et al., 2009). The green LiDAR offers a cost and time-effective alternative to SoNAR for mapping shallow water depths less than 50m; however, the penetration of LiDAR laser is hindered by turbidity in water depth greater than 35m (Costa et al., 2009). Bailly et al. (2010) assessed the accuracy of LiDAR bathymetric data collected for shallow waters and pointed out that the accuracy of river bottom elevation decreases with the

increase in river depth. The same author demonstrated that a continuous terrain model for shallow waters could be created using LiDAR elevation data but overlooked the validity of the same for deep river waters.

Multibeam SoNAR is a practical survey tool for capturing bathymetric data in deep navigable rivers (Kinzel et al., 2013). Costa et al. (2009) compared airborne LiDAR and ship-based multi-beam SoNAR survey results and found SoNAR depths to be consistently deeper than LiDAR depths, providing more details about the seafloor.

2.2.2 Empirical methods

Apart from hydrographic surveys and remote sensing methods, many researchers have also developed theoretical models and empirical methods to estimate river channel bathymetry. Yoon et al. (2012) estimated river bathymetry by assimilating the Surface Water and Ocean Topography (SWOT) satellite observations into a hydrodynamic model, including water surface elevation and inundation area. Corum et al. (2015) presented a method to create a synthetic bathymetry using GIS and Hydraulic Modelling techniques, but with a condition of known discharge value at the time of DEM data acquisition. Farina et al. (2015) developed a method for reconstructing a cross-section profile based on the maximum entropy principle. Lai et al. (2018) introduced an algorithm to generate a terrain model from streamlines of the river using elliptic and Laplace equations. The algorithm can generate a continuous river geometry, but it still requires physically measured cross-sections as input parameters. Also, it is unclear how the algorithm would tackle the challenging geometries of complex river systems such as braided river reaches and junctions. Bures et al. (2019) used the Machine Learning method- Random Forest (RF) for mathematical representation of river bathymetry. The model is useful when bathymetric measurements are not available. Park et al. (2020) proposed a method to estimate the bathymetry of turbid-water floodplains from historical inundation frequency data. Regardless of which method is considered for estimating river bathymetry, it will still be an approximation rather than detailed bathymetry and needs to be integrated with existing topographic DEM to generate a seamless terrain model.

2.3 Need for Topobathymetry DEM

An integrated terrain model consisting of airborne LiDAR-derived topography and bathymetry measurements can effectively improve the flood inundation extent (Chen et al., 2018). Generating an integrated Topobathymetry DEM (TB-DEM) is not a new concept. Many studies have developed TB-DEMs using different methods and for different purposes. Quadros et al. (2008) provided an early account of integrating topographic and bathymetric data and found the following key challenges: (1) The elevation information from different datasets may relate to a different datum, affecting their integration. (2) Fluctuations in water levels can affect both topographic and bathymetric data extents and may also result in significant data gaps.

Wilson & Power (2018) described an approach for generating seamless bathymetry and topography datasets at a small scale (1:25,000 or higher). The authors interpolated point elevation data at two instances: before and after integrating bathymetry and topography datasets. Numerous interpolations, especially the conversion of topographic raster DEM to point data and the subsequent interpolation back to raster data, drastically reduces the accuracy of upland terrain features captured in a LiDAR survey. Such a terrain modelling approach is suitable for morphological studies and coastal modelling at a regional scale but may not be better for localized urban areas (Wilson & Power, 2018).

National Oceanic and Atmospheric Administration (NOAA) has developed the Experimental Advanced Airborne Research Lidar (EAARL) sensor, which uses a green-wavelength LiDAR to map bathymetry, topography, and vegetation at once. The EAARL system can capture very accurate elevations for floodplains; however, the riverbed and bank features may not be accurately mapped if the turbidity of channel water is within the range of 4.2-19.3 NTU (Skinner, 2009). The EAARL-B system (newer version of EAARL) provides quality bathymetric data similar to multi-beam SoNAR, but its applicability is limited to the shallow gravel-bed river with no turbidity (Kinzel et al., 2013).

Danielson et al. (2016) presented a methodology for developing coastal TB-DEMs using a point cloud of topographic and bathymetric data. The method relies on the vertical datum transformations embedded into spatially consistent interpolation (gridding) techniques. It is applicable when the point cloud (raw) data is accessible. Falcão et al. (2016) interpolated cross-section data using thalweg, ancillary lines and the riverbank lines extracted from DEM to generate bathymetry. McGrath et al. (2017) also demonstrated a similar approach. Loftis et al. (2016) demonstrated the utility of incorporating LiDAR measurements into TB-DEM using a hydrodynamic sub-grid model. The model was developed using bathymetric point data and LiDAR point cloud data.

Based on the studies focused on TB-DEM so far, it can be stated that most of the existing methods for generating an integrated terrain model demand a certain quantity and quality of data that are generally not available in the public domain. With the development of LiDAR-based aerial surveys, high-resolution topographic DEMs are increasingly becoming available in many countries. Also, high-precision hydrography is present for most of the world, where extensive commercial navigation occurs in restricted waters (Journault et al., 2012). However, bathymetric information for rivers is sparsely available in the public domain.

2.4 Crowdsourced bathymetry: A way forward

A few private entities are now providing commercial maritime navigation services through their proprietary digital platforms. Using these navigation services, the ‘crowd’ regularly measures depth and location data from echo sounders and GPS installed on their boats or vessels. This data is collected, stored, and processed by the service provider to improve the navigation services. Consequently, the depth measurements are utilized to prepare the bathymetry data layer, often stored in proprietary data formats and usually not available in the public domain. Many governments and private organizations are developing collaborative measures for gathering and producing crowdsourced bathymetry datasets. For example, the International Hydrographic Organization (IHO) hosts a Data Centre for Digital Bathymetry to share depth data contributed by the mariners. The

Canadian Hydrographic Service (CHS), in its *Strategic Directions and Quality Policy 2018/28*, committed to increasing the use of crowdsourced bathymetry by developing and implementing a business model based on hydrospatial digital data (DFO, 2018).

These efforts indicate the possibility of high-quality bathymetric information, not just for oceans but also for rivers and lakes, becoming available in the coming years. With that, it is also expected that crowdsourced bathymetry will help to improve the hydraulic modelling studies. For instance, to measure the change in river bedform, the rate of collecting bathymetry data should be equal to or greater than the pace of bedform migration and seasonal change (Wang et al., 2019). The crowdsourced bathymetry, routinely updated as new information is gathered, can be a viable option for historical modelling and change detection studies.

Chapter 3:

Study Area and Materials

The area of interest (AOI) is the upstream of Montreal Island between 50,19,323m and 50,48,215m North and 2,35,600m and 2,90,775m East (Figure-2) in the Modified Transverse Mercator (MTM) coordinate system. A part of AOI is within the fluvial section of the St Lawrence River at Montreal City. The other part lies between the Ottawa River, the Lac des Deux Montagnes, and the Prairies River. The Beauharnois Dam and the Carillon Dam forms the upper boundaries of the AOI, respectively. The Rapids of Lachine on the St Lawrence River and the Grand Moulin Dam downstream of Lac des Deux Montagnes form the lower boundaries of the AOI.

St Lawrence river, the gateway to the heart of the North American continent, is the third-largest river system in North America after the Mississippi and Mackenzie river systems. Flowing from the Great Lakes to the Atlantic Ocean, the St Lawrence River drains more than 25% of the world's freshwater reserves. The main stem of St. Lawrence begins at the outlet of Lake Ontario and flows through four sections before reaching the Gulf of St. Lawrence: fluvial section, fluvial estuary, upper estuary, and lower estuary. From Lake Ontario to the end of the lower estuary, the river drops about an average of ~14 cm/km. It includes uppermost braided regions, constricted channels, rapids, modest floodplain areas and natural fluvial lakes (Benke & Cushing, 2005). The fluvial section of the St Lawrence River, which is entirely freshwater and non-tidal, is 655 km long, and it flows from Kingston, Ontario, to Lac Saint-Pierre near Trois-Rivières, Quebec (Gouvernement du Québec, 2021). The St. Lawrence upper estuary is a transition zone between fluvial (freshwater) and marine (saltwater) environments. In this zone, the tidal currents and wind cause mixing of the water of St. Lawrence tributaries with saltwater from the Gulf.

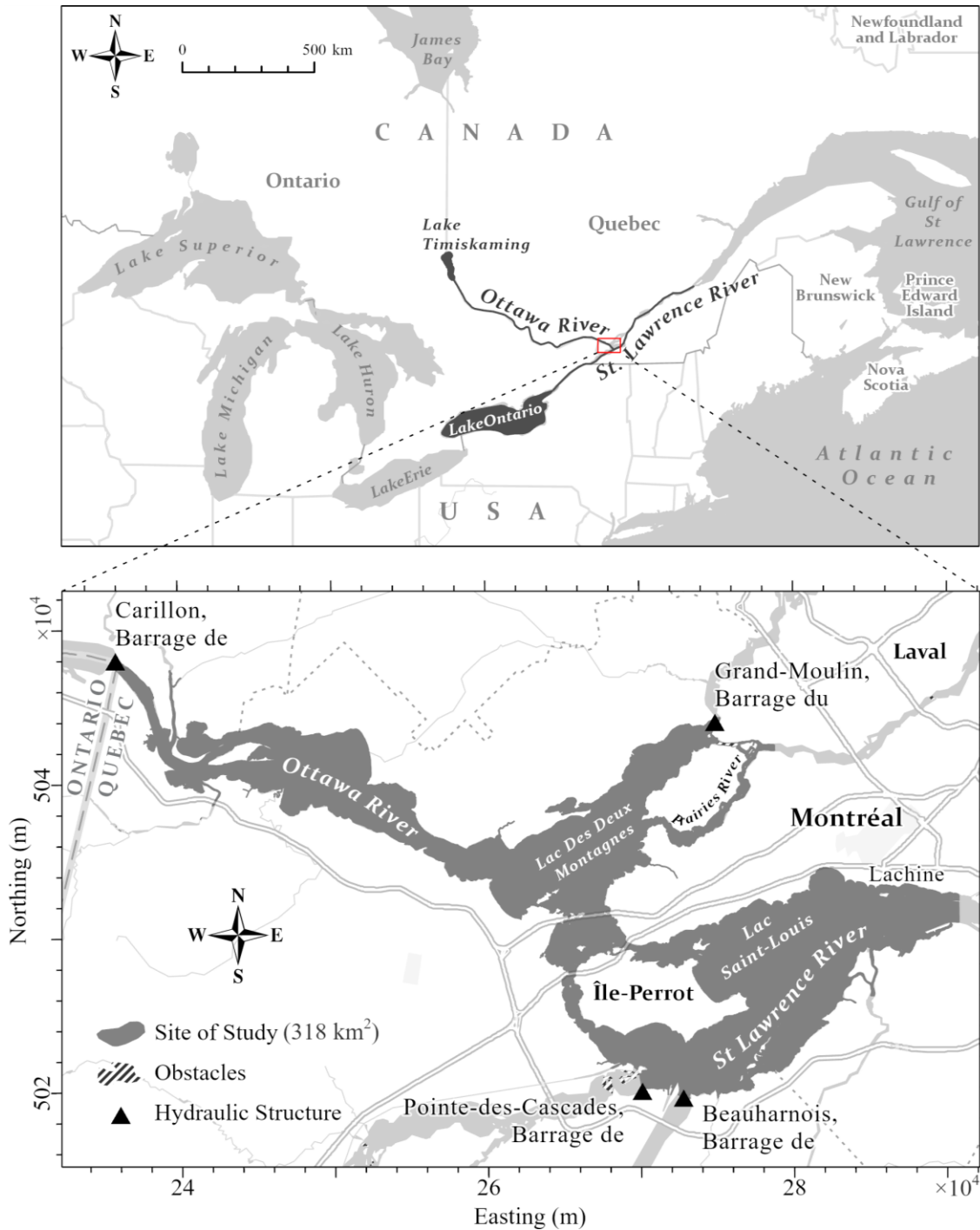


Figure-2: Location of the study area on the upstream of Montreal Island

The Beauharnois Dam near Montreal is a run-of-the-river type hydropower generating facility that draws 84% of the St Lawrence River's flow to pass through the power station and results in hydrodynamic alterations to nearby fluvial lakes and riverbed (Benke & Cushing, 2005).

Originating from Lake Timiskaming, the Ottawa River flows 1271 km to its confluence with the St Lawrence River near the Montreal archipelago. The Ottawa River channel is mostly naturally constricted and slopes about 36 cm/km. It is the largest tributary of the fluvial section of St. Lawrence River (Benke & Cushing, 2005). The Carillon Dam, located on the Ottawa River about 50 km upstream of Montreal Island, is also a run-of-the-river hydropower plant. As situated near the mouth of the Ottawa River, the dam observes a considerable volume of water with a mean flow rate of 1985 m³/s (ORRPB, 2021), reaching up to and beyond 8000 m³/s during the spring freshet (Ottawa Riverkeeper, 2021).

The AOI presents a complex case of a braided river system that includes two fluvial lakes, two major and a minor river section, convergence-divergence of water masses, rapids, and large hydraulic structures in the vicinity. The site also includes several areas, including Île-Perrot, which have observed significant flooding issues in recent years. From a perspective of hydraulic modelling, there is a need to study the complexity of channel geometry and explore 2D terrain modelling approaches that improve flood inundation estimates. The site highlights most of the challenges that typically occur in generating a hydrologically correct DEM and better represents the need to adopt a seamless DEM for 2D river modelling. The output from this study would also be helpful for researchers to study non-technical issues such as the impact of floods, safety of hydraulic structures and susceptibility to geomorphologic changes.

The DEMs available at the highest resolution were collected separately from each provincial government's data repository. In Quebec, the Ministry des Forêts, de la Faune et des Parcs (MFFP) disseminates LiDAR-derived products via its open data hub – *Données Québec*, including a digital elevation model with a spatial resolution of 1m. The raster grid DEM uses NAD83 (CSRS) as a geodetic reference system, and it provides altitudes in meters above mean sea level. The elevation stored in raster cells corresponds to linear interpolation of the triangulated irregular network (TIN) created from the LiDAR point cloud.

A small part of AOI lies within the boundary of Ontario. The Ministry of Natural Resources and Forestry (MNR), Government of Ontario, via its geospatial data portal – *Ontario GeoHub*, provides access to the Imagery-derived DEM. It is a 2m raster elevation product generated from the Ontario Classified Point Cloud (Imagery-Derived) data via a pixel-autocorrelation of the stereo aerial photography. Though DEM is not entirely a bare-earth elevation raster, it is only used to complete the overall AOI footprint and does not contribute to the main river channel area, which is the primary focus of this study.

Navionics[®] manufactures digital navigational charts of marine areas, lakes, rivers and provides navigation services to its subscribers. It provides crowdsourced content layers packaged with navigation aids and a variety of edits that are updated daily. SonarChart[™] is one such layer that is continuously updated using millions of sonar logs contributed by the users. Navionics also offers an online Chart Viewer, allowing free viewing access to their different chart information. The sonar bathymetry information for the entire AOI is sourced from this Chart Viewer. It should be noted that this study uses the finished bathymetry product, namely SonarChart[™], which has already undergone preliminary processes to aggregate the crowdsourced sonar logs. As such, the users of SonarChart[™] have no control over these preliminary processes because the information is distributed to them under proprietary licenses.

Natural Resource Canada produce digital cartographic reference product, namely CanVec, which provides various topographic information in vector feature formats. The hydrographic feature package of the CanVec database includes vector shapefiles of watercourses, water linear flow segments, hydrographic obstacles, waterbodies, permanent snow and ice features, water wells and springs. The CanVec waterbody feature layer is extensively used in this study for clipping GIS data and restricting the processing extent of various geoprocessing tools.

CHS has created Non-Navigational Bathymetric Data products, also known as NONNA-10 and NONNA-100, representing the validated digital bathymetric raster data at a resolution of 10 meters and 100 meters, respectively. Released first in October 2018,

the database is still transforming and getting frequent updates. As a result, the current data has considerable gaps, especially in the AOI (Figure-17b, 17c), either due to the non-surveyed area or delay in digitizing legacy data. Nevertheless, both NONNA-10 and NONNA-100 bathymetric data have been used in this study for external validation purposes only. The sources of data used in this study are summarised as follows:

Table 1: Sources of topographic and bathymetric data used in this study

Data type	Product name	Sources
LiDAR-derived DEM (1-m resolution)	-	Données Québec
Imagery-derived DEM (2-m resolution)	-	Ontario GeoHub
Sonar Bathymetry	SonarChart	Navionics [®]
Hydrographic variables	CanVec	NRCan
Reference Bathymetry Data	NONNA-10, NONNA-100	CHS

Chapter 4:

Methodology

The methodology adopted for this study is composed of the following four components. The overall process flow encompassing the practical components is described in Figure-3.

- (1) Developing a simple approach for integrating topographic and bathymetric information
- (2) Constructing a bathymetry DEM from crowdsourced data (Figure-3: Stage-1,2)
- (3) Making the Topographic and Bathymetric DEMs compatible for seamless integration (Figure-3: Stage-3,4)
- (4) Creating an integrated Topobathymetry DEM (Figure-3: Stage-5)

4.1 Superposition of topographic and bathymetric data

Airborne LiDAR surveys typically do not capture riverbed geometry wholly and accurately, and in the same way, hydrographic surveys cannot map overbank terrestrial geometry beyond a certain limited extent. The LiDAR survey produces high-density point-elevations, which in turn help generate a high-resolution raster grid DEM. Contrarily, single-beam and multi-beam SoNAR-based hydrographic surveys record relatively low-density point-elevations. Therefore, hydrographic survey output usually is not outright adequate for generating high-resolution raster-grid DEMs.

The study proposes a superposition-based approach using additivity property for combining topographic and bathymetric information and generate a continuous terrain surface. It utilizes terrestrial and bathymetric elevation information that is typically available in a raster grid format. The LiDAR DEM is superpositioned on top of the bathymetry DEM by a numerical addition of stored elevation values respectively on a cell-by-cell basis. Such numerical addition does not alter the resolution and accuracy of the

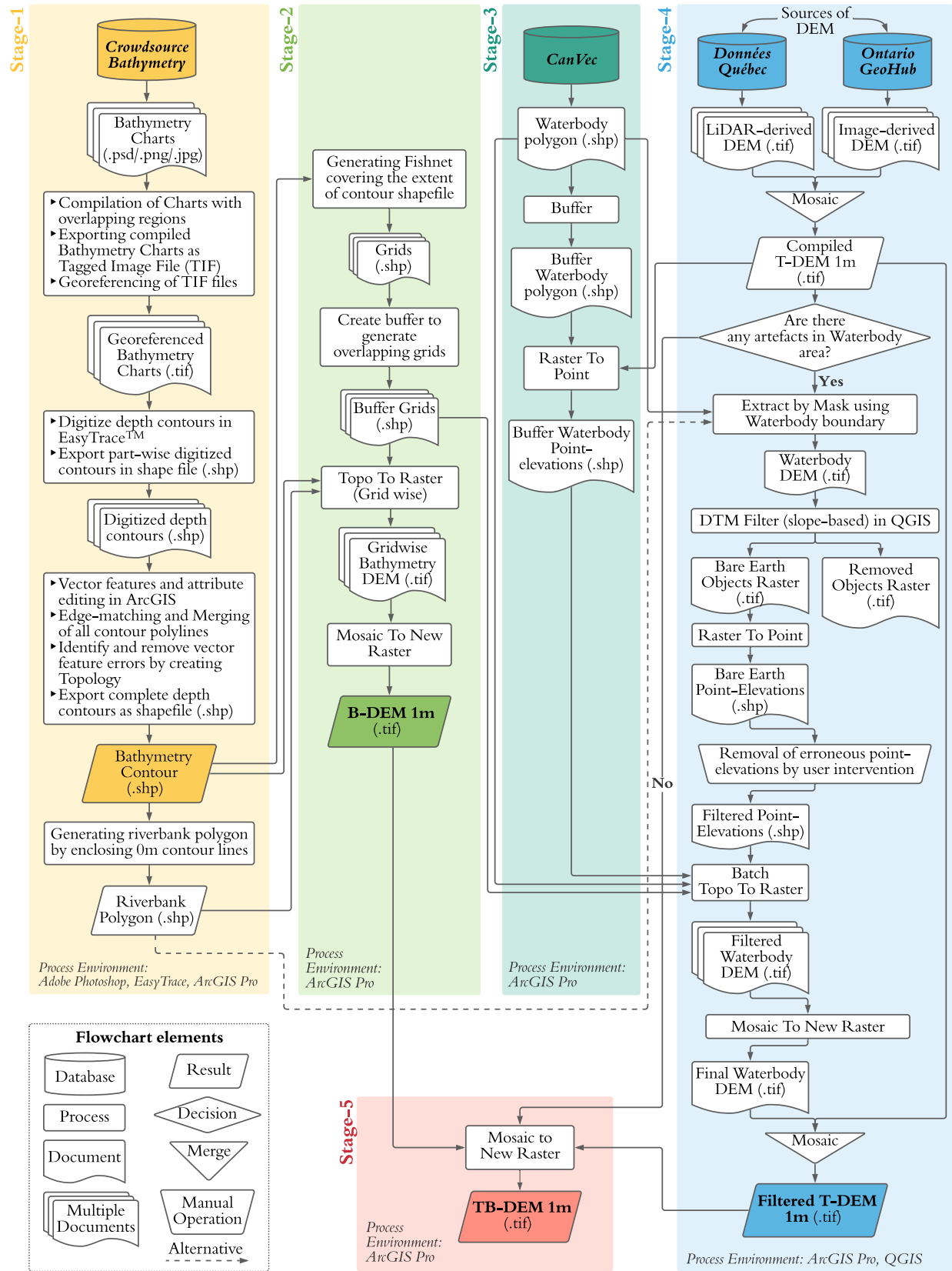


Figure-3: Process flow chart for generating Topobathymetry DEM

LiDAR DEM but instead updates the channel bathymetry, which is not usually recorded by the airborne LiDAR sensors. However, superposition accuracy would depend on the choice of common feature acting as a basis for the numerical addition of riverbed elevation values.

It is worth mentioning that a raster grid DEM stores elevation values measured from a particular datum. Since both topography and bathymetry information refer to separate datum references, one dataset needs to be changed to match the other. It is convenient and preferable to convert bathymetry information because they typically refer to a temporary datum, meaning that the riverbed elevation is denoted as depth measured from water surface elevation (WSE) (Figure-4b). The actual riverbed elevation can be obtained by deducting the water depth (generally referred from a navigation chart or hydrographic survey) from known water surface elevation (Legleiter, 2021).

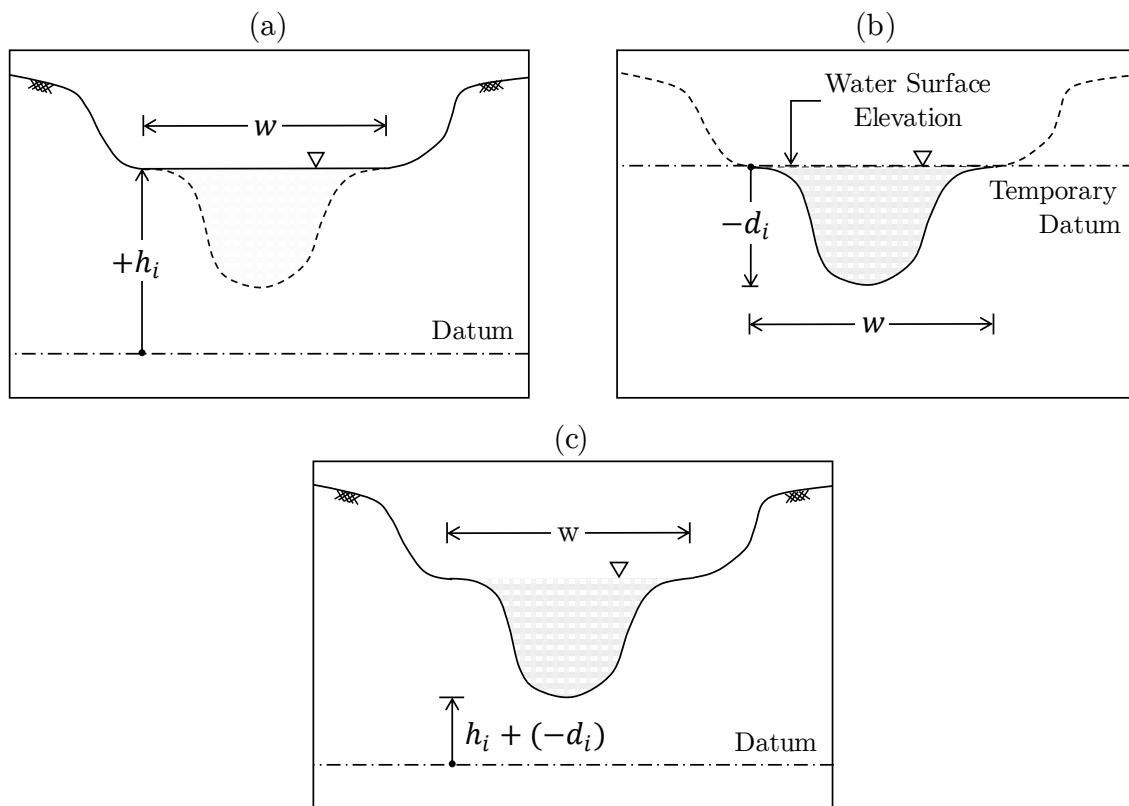


Figure-4: Schematic representation of a channel cross-section showing the superposition of LiDAR-derived topography onto SoNAR-derived bathymetry

Initially, an inverted Bathymetry DEM is created using depth measurements, and then it is superpositioned onto the LiDAR DEM. The main advantage of using the inverted bathymetry raster is that the depth measurements are numerically adjusted with elevation values conforming to LiDAR DEM. Figure-4a and 4b show a schematic cross-section of a river channel recorded in LiDAR DEM and Bathymetry DEM. The elevation value of cell i of the integrated Topobathymetry DEM (TB-DEM) shall be calculated using the following equation:

$$Z_i = h_i + (-d_i) \quad \text{Eq. 1}$$

where h_i denote the elevation value of cell i from the LiDAR DEM, and d_i denote the cell depth from bathymetry DEM.

The topography represents mainly the earth's geological features which are fundamentally static, whereas the bathymetry represents hydrological features, i.e. waterbodies that are somewhat dynamic. A LiDAR-derived DEM represents the dynamic nature of WSE as a static feature using elevation values. WSE can be the common feature that is often reflected in both topographic and hydrographic surveys. However, there are two prerequisites for WSE to be considered as a common feature for integrating topography and bathymetry:

- (1) Temporal prerequisite: Topographic and hydrographic surveys should be conducted at an exact point in time.
- (2) Spatial prerequisite: The aerial extent of the waterbody in both datasets should be identical.

The temporal prerequisite is rarely fulfilled in practice, given the cost and operational complexities of both topographic and hydrographic surveys. However, the spatial prerequisite can be established by careful attention to the formation of riverbank lines and adjusting them with the reference topographic data when necessary.

4.2 Generating river bathymetry DEM

Navionics SonarChart displays bathymetric information in the form of riverbed contours at an interval of 1 ft (= 0.3048 m). Since the online chart viewer does not provide download access to raw data, the bathymetric information was collected by capturing multiple image tiles at maximum zoom level covering the entire AOI and compiling them together in the image editing program Adobe Photoshop (Figure-5) to generate a complete digital canvas. The compilation process demands greater attention to match the edges of each image tile with its surrounding tiles and adjusting each layer's opacity to ensure a proper overlapping of contour lines. The resolution of the digital canvas is kept at 300 Pixels/Inch to retain the maximum resolution of image tiles. The process is similarly applicable if the bathymetry charts are in paper format, which requires an additional prior step of scanning the paper charts into a digital raster image format.

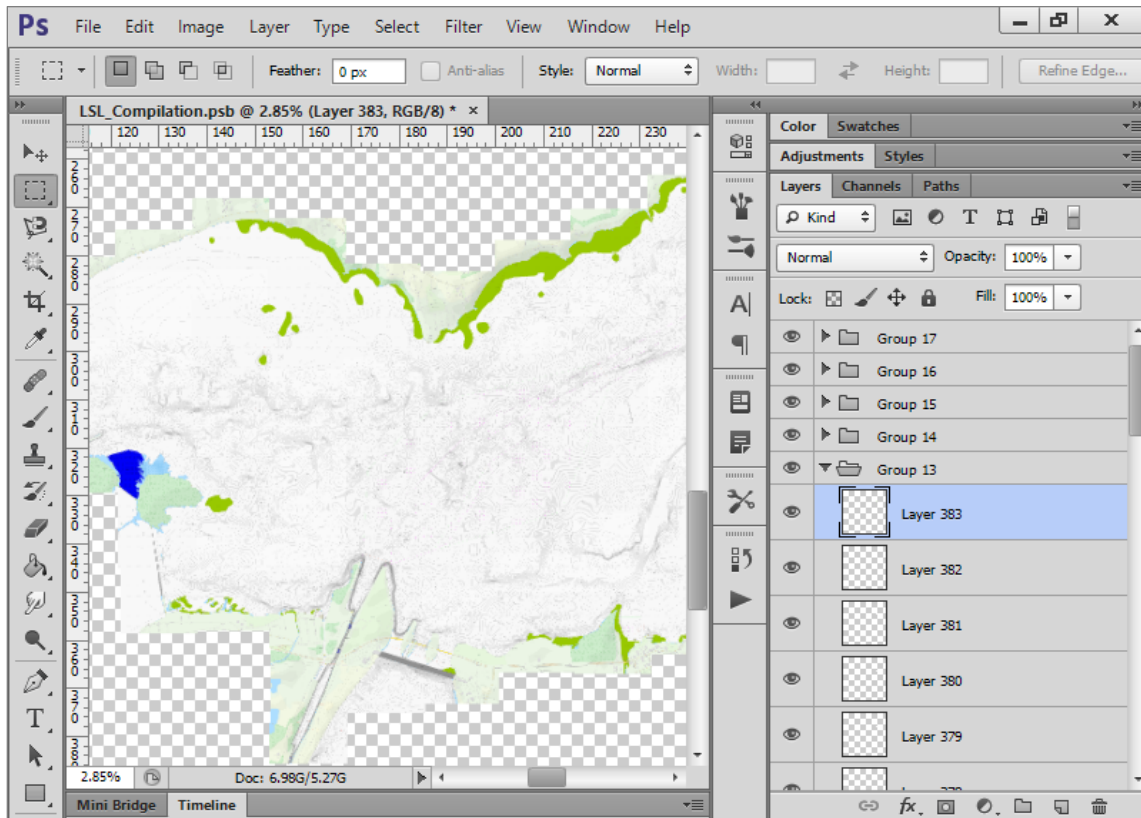


Figure-5: Using image editing program to compile multiple image tiles and generating digital canvas of bathymetry chart

(Program source: <https://www.adobe.com/products/photoshop.html>)

A complete and georeferenced version of the bathymetry chart is essential for tracing riverbed contour features. First, the compiled digital image of the bathymetry chart is georeferenced with satellite imagery in ArcGIS using the image-to-image georeferencing technique (Figure-6). Next, the raster features of the georeferenced bathymetry chart are converted into vector features using the digitization program – EasyTrace Pro 8.65. It should be noted that the file format of the georeferenced bathymetry chart has to be compatible with the digitization program. Some digitization programs do not often support the raster dataset having pixel depth higher than 8 BIT. Therefore, the georeferenced bathymetry chart should be exported from higher pixel depths (32 BIT or 16 BIT) to lower pixel depth (preferably 8 BIT) using the current renderer option in ArcGIS.

The digitized vector features do not hold any attribute values at this stage, i.e. depth measurements, and require manual attribute editing in ArcGIS. A topology query was also set up in ArcGIS to identify topological errors associated with vector features such as *overlap*, *self-intersect* and *dangles*. After addressing all errors and editing depth contours, the vector features are exported in a shapefile (.shp) format. Due to the file size limitations of image editing and vectorizer programs, the digital canvas of the bathymetry chart was initially divided into several parts (Figure-6a, 6b and 6c) for convenient georeferencing and vectorization. These parts were afterwards merged to create a single raster (Figure-7b) and vector feature file (Figure-7c), respectively.

The outermost contour lines have a depth value of 0m and represent the riverbank lines. An accurate riverbank line is an essential component for constraining interpolation (Fregoso et al., 2017). Therefore, a riverbank polygon is created by merging these riverbank lines, enclosing all water bodies within the AOI.

The contour shapefile provides bathymetry information only where contour polylines exist, not between the contour polylines (Figure-7c). So, a continuous raster grid DEM is generated from the irregularly spaced contour elevation data using *Topo To Raster* interpolation tool in ArcGIS (Figure-7d). The tool works precisely with contour elevation data and generates a hydrologically correct raster grid DEM. Here, it should be noted that

hydrologically corrected DEM is an essential step for many hydraulic and hydrologic modelling studies. Callow et al. (2007) analyzed the impact of three hydrological correction methods (*Stream burning*, *Agree.aml* and *ANUDEM*) and found ANUDEM producing the expected result more adequately. *Topo To Raster* is based on the ANUDEM v5.3 program developed by Michael Hutchinson. A primary disadvantage of other general-purpose interpolation techniques such as *Inverse Distance Weighted*, *Kriging*, *Natural neighbour*,

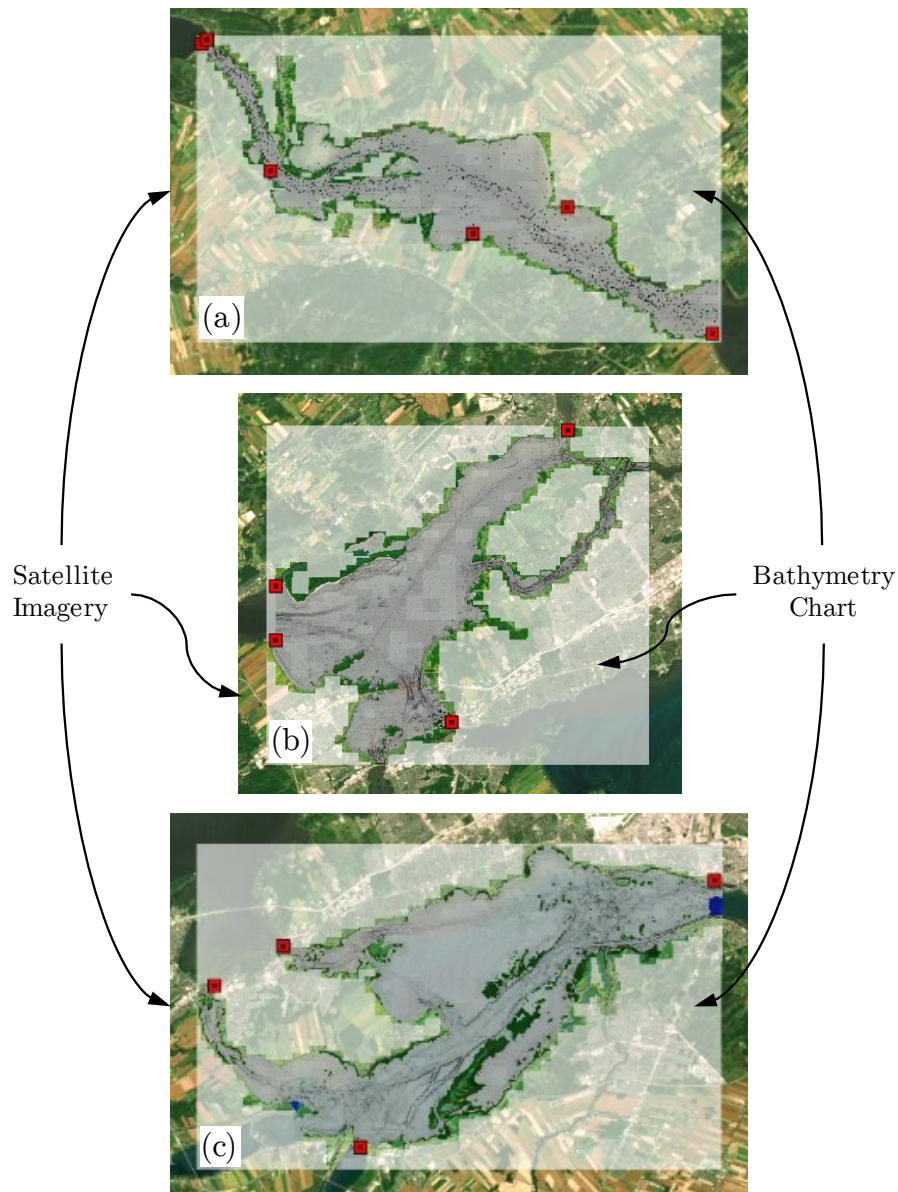


Figure-6: Georeferencing part-wise bathymetry chart with satellite imagery in ArcGIS: (a) Ottawa River chart using six links, (b) Lac des Deux Montagne and Prairies River chart using four links, (c) St Lawrence River and Lac Saint-Louis chart using four links.

and *Spline* is that they introduce spurious sinks or pits. In comparison, the drainage enforcement algorithm of the ANUDEM program ensures better shape and drainage structure by automatically removing the sinks, making the interpolated DEM much more suitable for hydrological applications (Hutchinson, 2011).

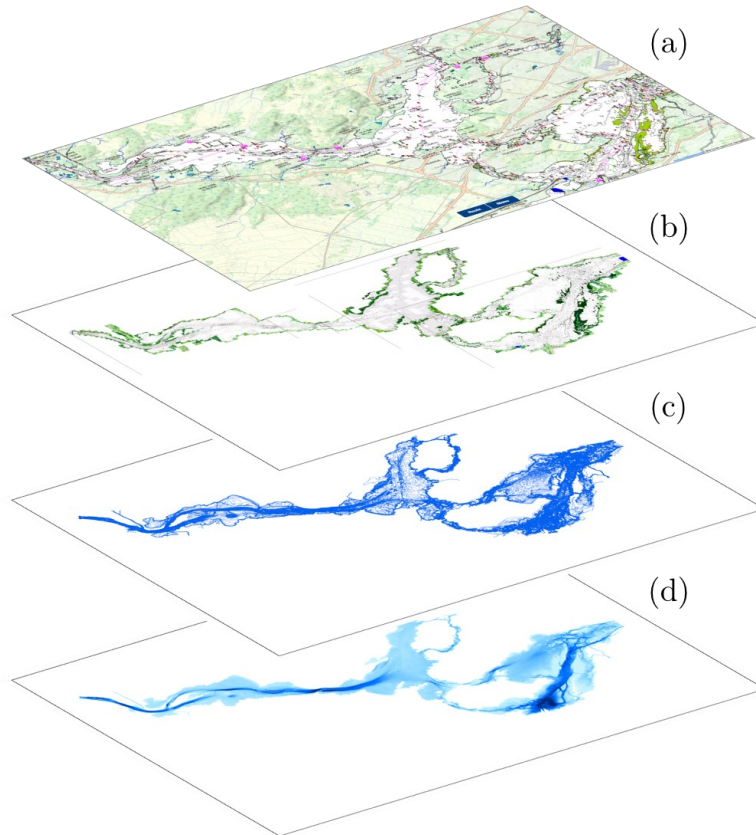


Figure-7: Layers involved in the generation of Bathymetry DEM: (a) Navionics bathymetry chart, (b) Georeferenced bathymetry chart, (c) Depth contours (vector features), and (d) Interpolated bathymetry raster

Topo To Raster interpolation tool requires at least two primary types of input data for interpolating bathymetry: (1) contour data (as polyline feature class) and (2) boundary data (feature class containing a polygon). Here, the riverbank polygon is used as boundary data for clipping out water areas along the riverbank lines before the final output raster is generated. In other words, the cells in the interpolated raster outside this boundary are going to be *NoData*. Also, it is expected that the contour depth values will be interpolated only up to the riverbank line, which has a depth value of 0m. Therefore, the maximum z-value parameter is also set to 0m for the interpolation process.

Topo To Raster is a resource-intensive application, and therefore the tool cannot create large output rasters. Reducing the output cell size increases the output raster size considerably, especially when the AOI is already quite large and the desired cell size is 1m. Therefore, the AOI is divided into smaller overlapping grids (polygons), and the interpolation is performed in batch mode using each grid as a processing extent simultaneously (Figure-3, Stage-2). The multiple output rasters are then mosaicked together to create the Bathymetry DEM (B-DEM).

4.3 Pre-processing LiDAR-derived topography DEM

Quebec and Ontario's data repositories provide raster DEM tiles conforming to Canada's National Topographic System (NTS). Each tile is a different Tagged Image File Format (*TIFF* or *.tif*) available at a scale of 1:50,000. The DEM tiles covering the entire AOI were downloaded and mosaicked together to generate a single raster DEM.

DEM artefacts have more impact on the slope and can best be detected using a shaded relief of the DEM (Polidori & Hage, 2020). A visual inspection of the LiDAR DEM *hillshade* and *slope* revealed excessive surface roughness and artefacts present in the water body area of the DEM (Figure-8, 9 and 10). The proposed approach (Section 4.1) requires the LiDAR DEM to represent water surface elevation as precisely as observed in natural conditions. Any deviations in LiDAR elevation caused due to surface roughness or artefact, if not removed, would render the B-DEM erroneously during the superpositioning process.

The artefacts observed in Figure-8 have possibly been caused by the Delaunay triangulation of the LiDAR point cloud. It is a widely used surface modelling approach and requires high-density point elevation measurements. However, when merging two datasets having different point-elevation densities, the Delaunay Triangulation results in spurious but redundant triangles at the common boundary (Flanagin et al., 2008). These triangles, embedded in the DEM during its creation from LiDAR point cloud, do not represent the actual riverbank topography and may create inaccuracies in subsequent hydraulic models.

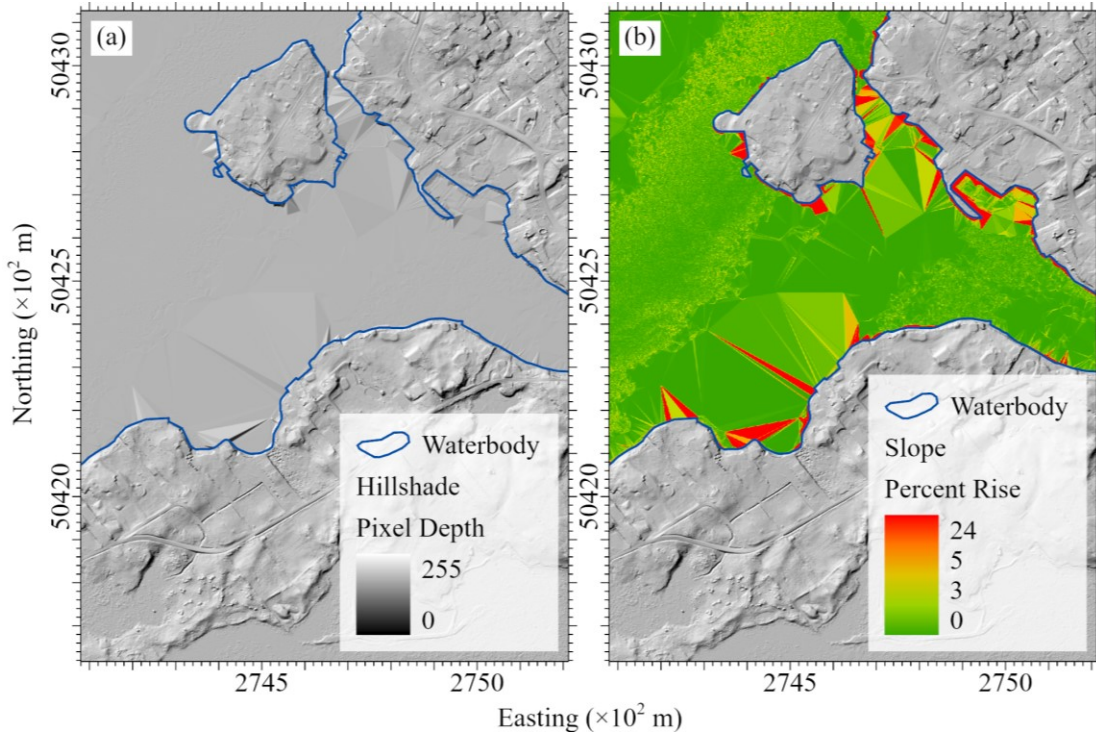


Figure-8: Detecting artefacts of Triangulation-based errors using hillshade and slope raster

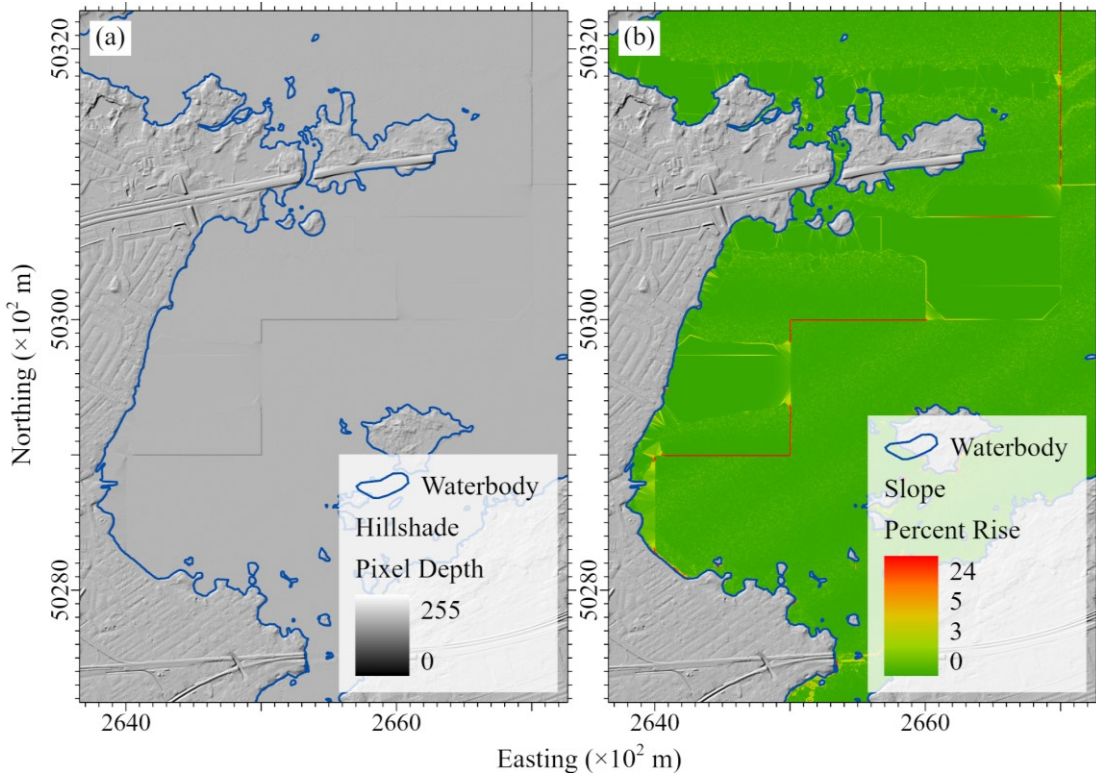


Figure-9: Detecting artefacts induced by the stitching of LiDAR survey grids using hillshade and slope raster

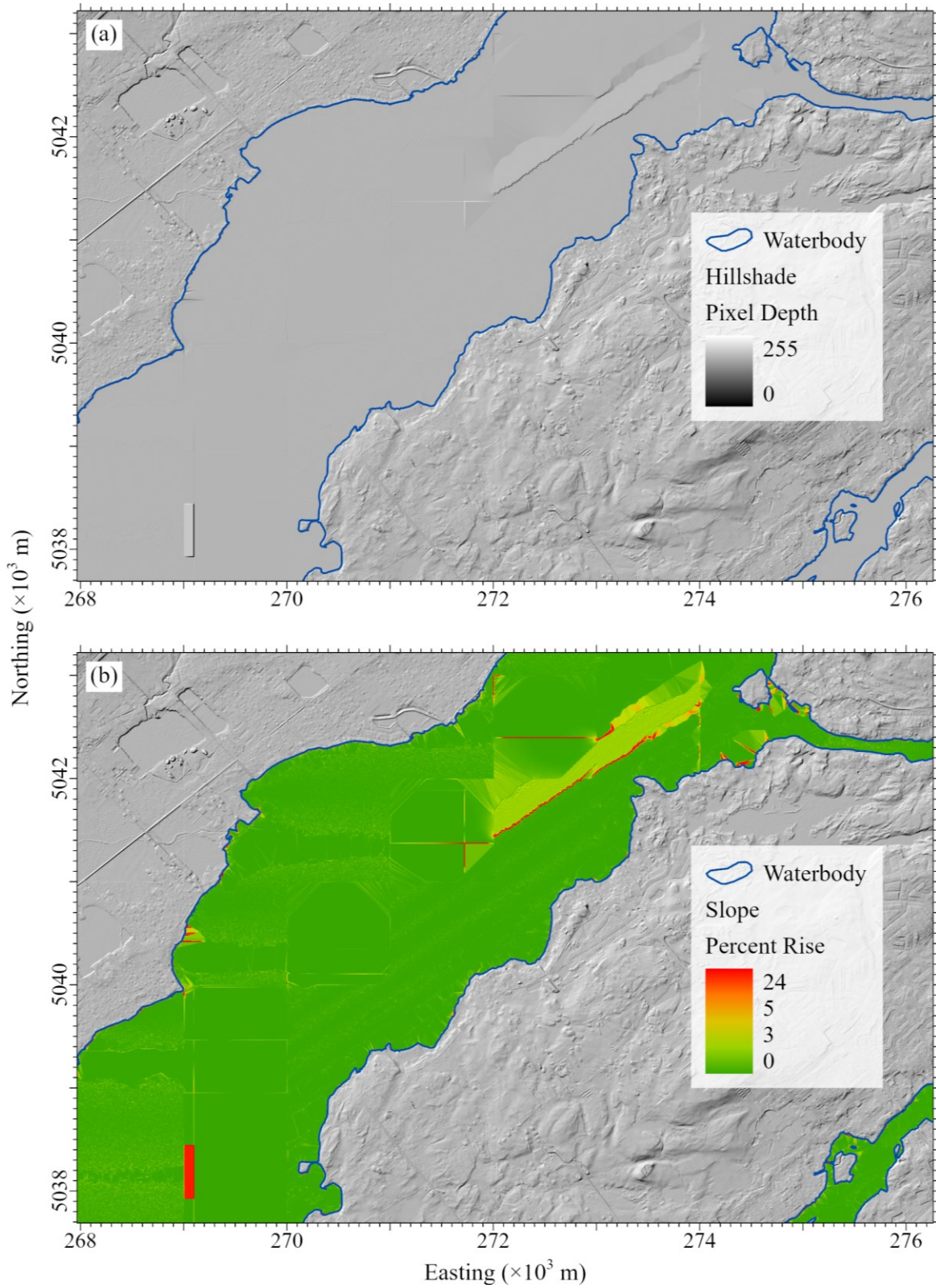


Figure-10: Detecting artefacts of Unnaturally steep and shallow ground features using hillshade and slope raster

A slope-based filtering procedure is applied to LiDAR DEM to avert unwanted rendering of the B-DEM. The filter classifies the LiDAR DEM cells into bare earth and object cells based on the acceptable height difference between the neighbouring cells (Vosselman, 2000). It is generally applied to a digital surface model (DSM) to filter the bare earth surface by systematically removing the canopy heights. However, for a similar purpose in this study, the same filter is applied locally to LiDAR DEM to remove cells that have unnatural heights or surface roughness only within the water body area.

The filtering procedure is carried out in QGIS using the SAGA-GIS Module of *DTM Filter (slope-based)*. The filter function determines the acceptable height difference based on the user-defined kernel search radius in cells. It can also be modified to match the AOI's overall slope by user-specified *approximate terrain slope* as an input parameter. This parameter filters out most errors and artefacts thoroughly. It should be noted that the filter is selectively applied only to the water body area to remove the artefacts. The rest of the LiDAR DEM consists of overbank regions that need not be filtered to preserve the upland topography. So, the waterbody area is extracted from the LiDAR DEM using the CanVec waterbody polygon before applying the filter. Here, the CanVec waterbody polygon is preferred for extracting the waterbody DEM so as to maintain consistency between the datasets published by the government agencies. After applying the filter, two mutually exclusive but collectively exhaustive raster files are created: (1) A bare waterbody raster file including only the anticipated WSE cells and (2) a removed object raster file leaving out the unwanted error cells.

The bare waterbody raster contains dispersed elevation cells, which require interpolation to fill the data gaps or voids using *Topo To Raster* interpolator. Any artefact that still exists even after applying the filter can be removed by manual intervention. It was observed that the artefacts such as sinks or depressions were not removed by the *DTM Filter (slope-based)* because the slope parameter appeared to be considering only the positive slope values, not the negative slope values. Therefore, the bare waterbody raster was converted to points, and the remaining artefact point features were removed manually.

Disparate multi-temporal sources of topography and bathymetry measurements result in conflicting overlap, which can be minimized using a buffer to ensure a seamless transition and preserve the nearshore features (Loftis et al., 2016). In addition, the elevation values interpolated near the riverbanks can be improved using a bank line *Buffer* during the interpolation process (Fregoso et al., 2017). Therefore, the interpolation is extended beyond the water body area by specifying an appropriate buffer distance (20m in this case) to allow for a smooth transitioning edge that blends well with the original LiDAR DEM (Figure-11). Again, the interpolation is performed in multiple grids using a batch process to generate the output rasters at a resolution as high as 1m. The final step is to update the filtered waterbody back into the original LiDAR DEM, thereby generating a smooth continuous Topography DEM (T-DEM) free from artefacts.

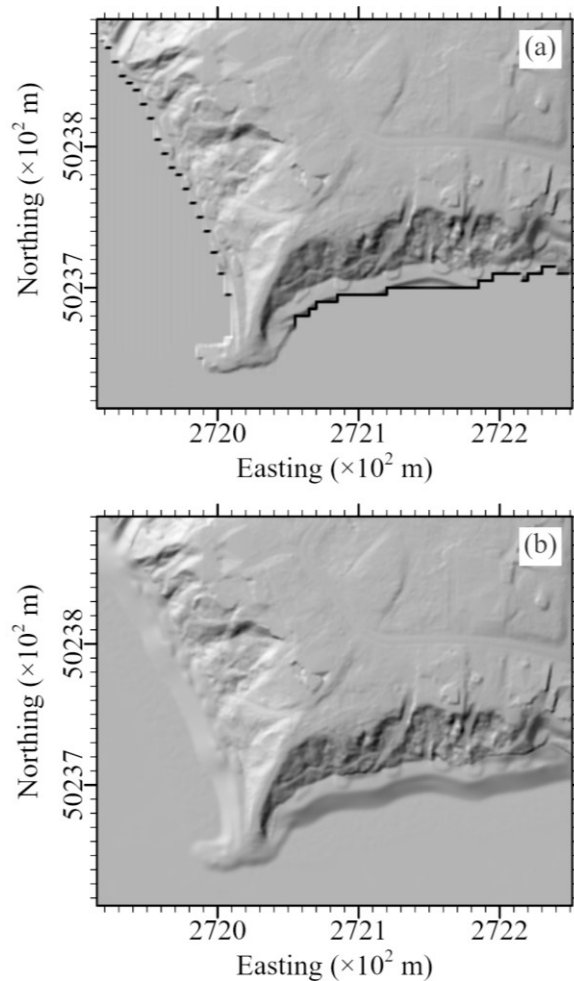


Figure-11: Terrain interpolation using point-elevations (a) without buffer and (b) with buffer (20m)

4.4 Generating Topobathymetry DEM

The Bathymetry DEM (B-DEM) is numerically added to the LiDAR-derived Topography DEM (T-DEM) to generate the combined Topobathymetry DEM (TB-DEM). The per-cell addition of elevation value is conducted using the *Mosaic To New Raster* tool with a *Sum* operator in ArcGIS. B-DEM is an inverted DEM and does not have any cell elevations outside the water body area. Therefore, when both T-DEM and B-DEM are added, the cell elevations of land area in the T-DEM remain unaffected by the statistical operation (Figure-12).

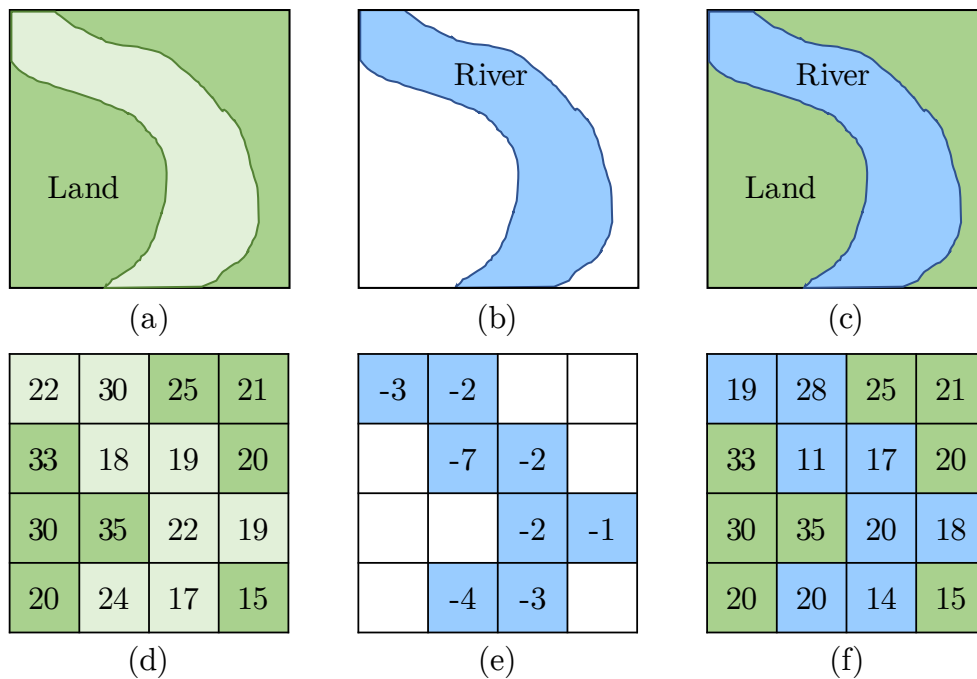


Figure-12: An illustration showing the superposition of (a) Topography on (b) Channel Bathymetry, giving the (c) combined Topobathymetry. The superpositioning adds elevation values from (d) LiDAR DEM to (e) Inverted Bathymetry DEM on a cell-by-cell basis resulting in a seamless (f) Topobathymetry DEM.

The final TB-DEM is a single-band raster file (*.tif*) with a cell size of 1-m \times 1-m. The *.tif* file is in the projected coordinate system of *NAD 1983 CSRS MTM 8*, also referred to as EPSG-2950. The raster has a pixel depth of 32-bit, and the cell values show altitudes in meters with reference to the geodetic vertical datum *NAD 1983 CSRS*. A 32-bit

encoding enables TB-DEM to represent negative float numbers, increasing the precision and elevation range of high accuracy DEM obtained by aerial photogrammetry or laser scanning (Polidori & Hage, 2020). However, 32-bit encoding and smaller cell size increase the file size massively, resulting in an uncompressed raster size of 6.57 gigabytes.

A thematic map depicting elevations from the final TB-DEM is shown in Figure-13. It can be seen from the map that the elevation information is continuous without any void, resulting in a seamless DEM. The map also includes ten selected cross-sections distributed across AOI showing different water bodies. The individual terrain profiles from T-DEM, B-DEM, and TB-DEM are shown in Figure-14. These terrain profiles show that the T-DEM, derived from the airborne LiDAR survey, did not capture any bathymetry. The constant elevation of T-DEM throughout the width of the river and lake water body also indicates that the artefacts have been successfully removed and now represents the uniformly flat water level. The smooth channel bathymetry profiles are attributed to the 1m spatial resolution of B-DEM. The superposition resulted in a seamless transition between B-DEM and T-DEM at riverbanks without changing the upland topography. It can be observed from the cross-sections that TB-DEM has retained the shape and slope of both T-DEM and B-DEM, respectively. Also, as seen in Figure-14, the intermittent bathymetry sections A-A, F-F and J-J blend well with the existing T-DEM.

The depth measurements from B-DEM are effectively transformed into elevation values conforming to LiDAR-derived T-DEM without needing the datum transformation. This is because the water surface elevation captured in LiDAR T-DEM becomes the basis for numerically adjusting depth measurements, and therefore, must be free from errors and artefacts.

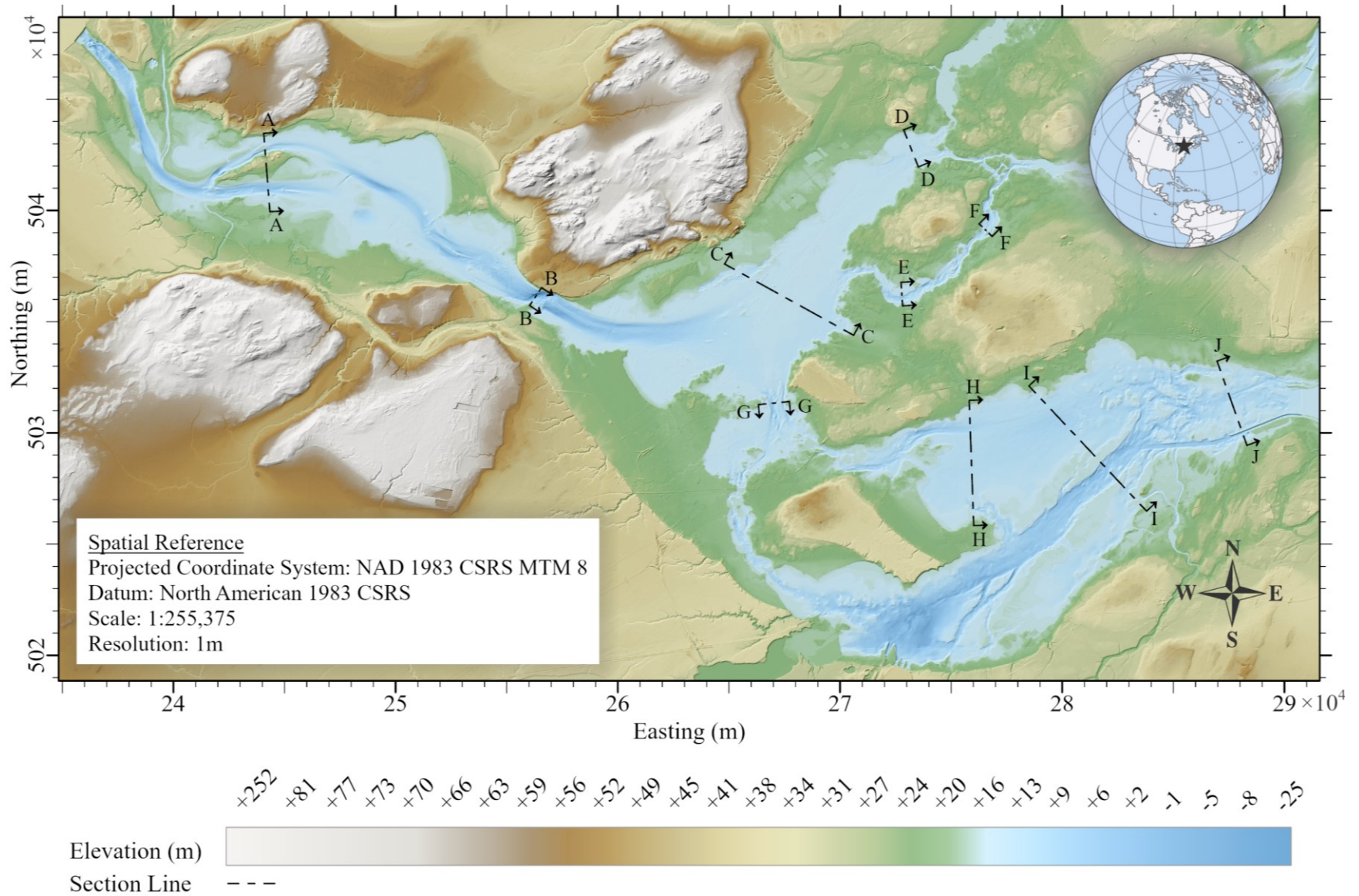


Figure-13: Seamless Topobathymetry DEM of the AOI at Montreal Island

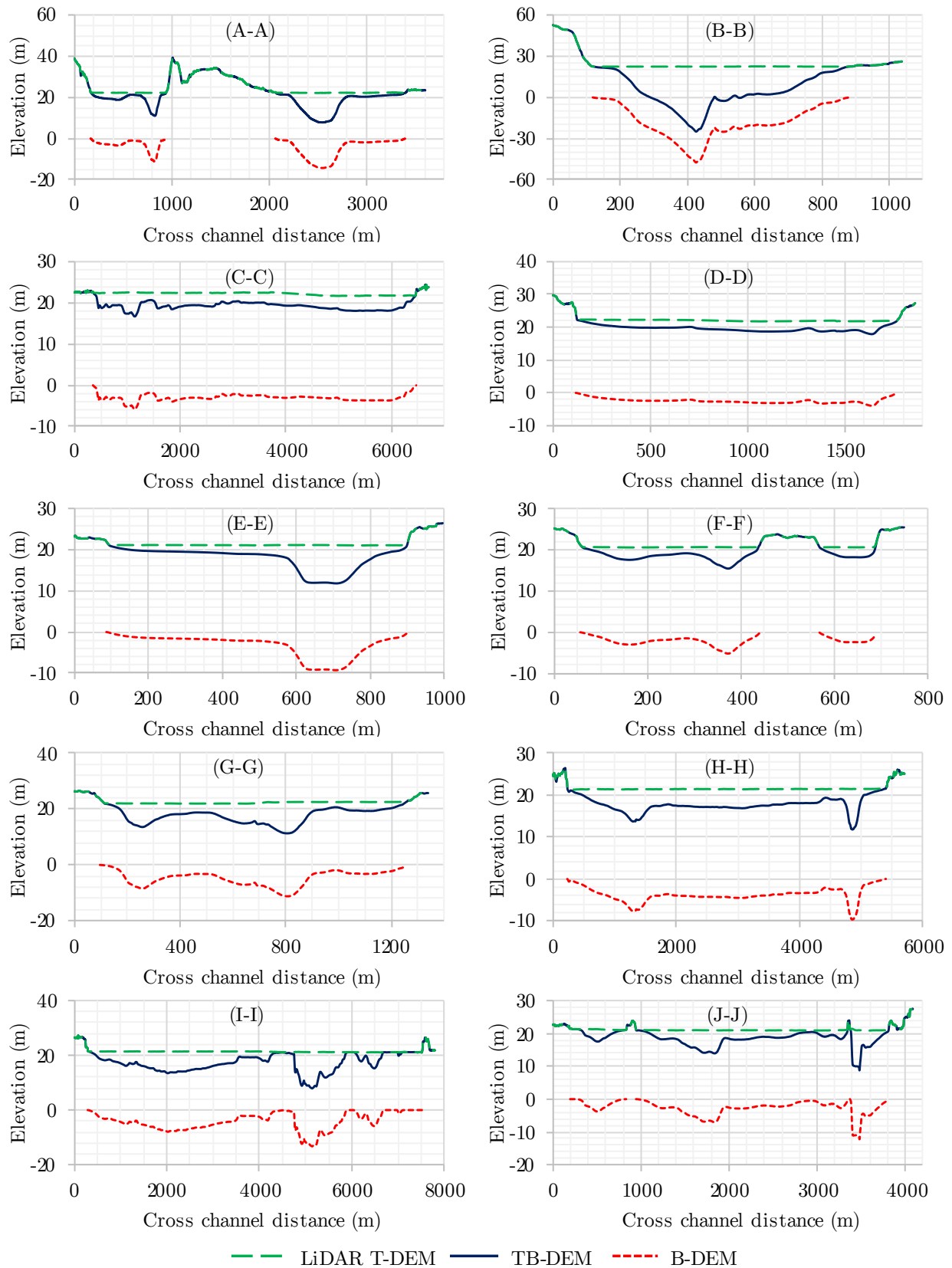


Figure-14: Selected cross-sections (A-A) to (J-J) showing different terrain profiles

Chapter 5:

Results and Validation

The DEMs used in hydraulic modelling should be verified based on ground measurements (Laks et al., 2017). However, this study relies entirely on the elevation information obtained from secondary data sources and has limited avenues for validating the Topobathymetry DEM. Furthermore, the accuracy of the integrated TB-DEM essentially depends on the individual accuracies of the input DEMs. Therefore, in the absence of ground control data, the TB-DEM accuracy assessment is conducted using internal and external validation approaches separately for T-DEM and B-DEM (Polidori & Hage, 2020).

According to NSSDA¹, the positional accuracy of a point on a map or in digital geospatial data should be tested and reported with respect to the georeferenced ground positions of higher accuracy. The dataset generated in this study is a seamless raster grid DEM having a horizontal resolution of 1m. So, ideally, the dataset coordinate values should be compared with an independent source having a resolution higher than 1m.

Regarding topographic data, it is assumed that the DEMs obtained from respective government agencies have previously fulfilled the required quality criteria as per the national standards. Therefore, LiDAR T-DEM does not necessarily require any further external validation; however, it was filtered to remove the artefacts, requiring internal validation pre and post-processing.

On the other hand, the crowdsourced bathymetry data was retrieved from Navionics' online chart viewer, and intrinsically, neither include ground control points nor any

¹ Published by the Federal Geographic Data Committee, c/o U.S. Geological Survey, the *National Standard for Spatial Data Accuracy* (NSSDA) provides a statistical and testing methodology for estimating positional accuracy of geospatial data.

metadata about the horizontal resolution and vertical accuracy. Therefore, the derived bathymetry raster needs to be validated internally and externally using other reference data sources. As of May 2021, only two bathymetric datasets were available in the public domain: NONNA-10 and NONNA-100 Bathymetric Data produced by CHS. These are non-navigational bathymetric datasets acquired using airborne LiDAR surveys and available in approximate 10m and 100m resolution, respectively. The NONNA products do not conform to a universal vertical datum but then provide depth values in negative numbers and elevation of some visible land as positive numbers (CHS, 2020). The intermediate results generated at different stages have been tested using the following internal and external validation techniques.

5.1 Internal Validation

5.1.1 Georeferencing of bathymetry charts

The georeferencing method should not warp or bend the bathymetry chart, i.e. the inbuilt contour information, beyond an extent because it may affect the surface parameters such as *slope* and *aspect* significantly. Therefore, the bathymetry charts are georeferenced using the *first-order polynomial transformation* method (also known as *affine*) since it only shifts, scales, and rotates the raster dataset and does not alter the footprint of depth contours (ESRI, 2018).

The bathymetry chart did not have adequate ground control points covering the AOI. Therefore, identifiable ground features such as a marina, dock, or edge of a hydraulic structure were used as control points to link the bathymetry chart with already georeferenced satellite imagery. The first-order polynomial transformation uses the following equation to transform a raster dataset:

$$x' = Ax + By + C \tag{Eq. 2}$$

$$y' = Dx + Ey + F \tag{Eq. 3}$$

where, x' is the horizontal value in coordinate space; y' is the vertical value in coordinate

space; A is the width of the cell in map units; B is a rotation term; C is the x' value of the center of the upper-left cell; D is a rotation term; E is the negative height of the cell in map units; F is the y' value of the center of the upper-left cell; x is the column count in image space; y is the row count in image space.

Using Eq. 2 and Eq. 3, the first-order polynomial transformation method maps each raster point to the target location with a minimum of three control points (ESRI, 2018). However, more than three links have been selected to map areas of the bathymetry chart accurately to their respective target locations (Table-2). The root mean squared error (RMSE) is induced due to mathematical transformation and does not imply inaccurate georeferencing. The accuracy of raster transformation has been validated by visual inspection, and it showed acceptable conformity throughout the AOI (Figure-6).

Table 2: Georeferencing links and errors

Bathymetry Chart Area	No. of Links	Total RMSE
St Lawrence River and Lac Saint-Louis	4	0.21616 (forward)
Lac des Deux Montagne and Prairies River	4	1.64507 (forward)
Ottawa River	6	3.88256 (forward)

Georeferencing a raster image introduces some errors, especially when the georeferenced image is further referred to for tracing information. However, the extent to which these errors propagate is not the primary objective of this study and, therefore, is not thoroughly investigated.

5.1.2 Visual inspection of Bathymetry DEM

Despite careful vectorization of contour information from bathymetry charts, a small probability that a wrong depth value may have been recorded on a correct contour line exists. These gross errors were identified by superimposing the contours generated from B-DEM onto the earlier digitized contours, using which the B-DEM was initially interpolated (Li et al., 2004). It should be noted that both contour datasets should have

the exact contour interval. The inconsistencies found at few locations in contour data were confirmed with the help of shaded relief of B-DEM. The mutations in contour lines were found to have occurred due to incorrect and inconsistent depth values associated with the respective contours. A few of such errors are highlighted in Figure-15. All such contour features have been edited with correct depth values, and the respective gross errors have also been rectified in the final B-DEM.

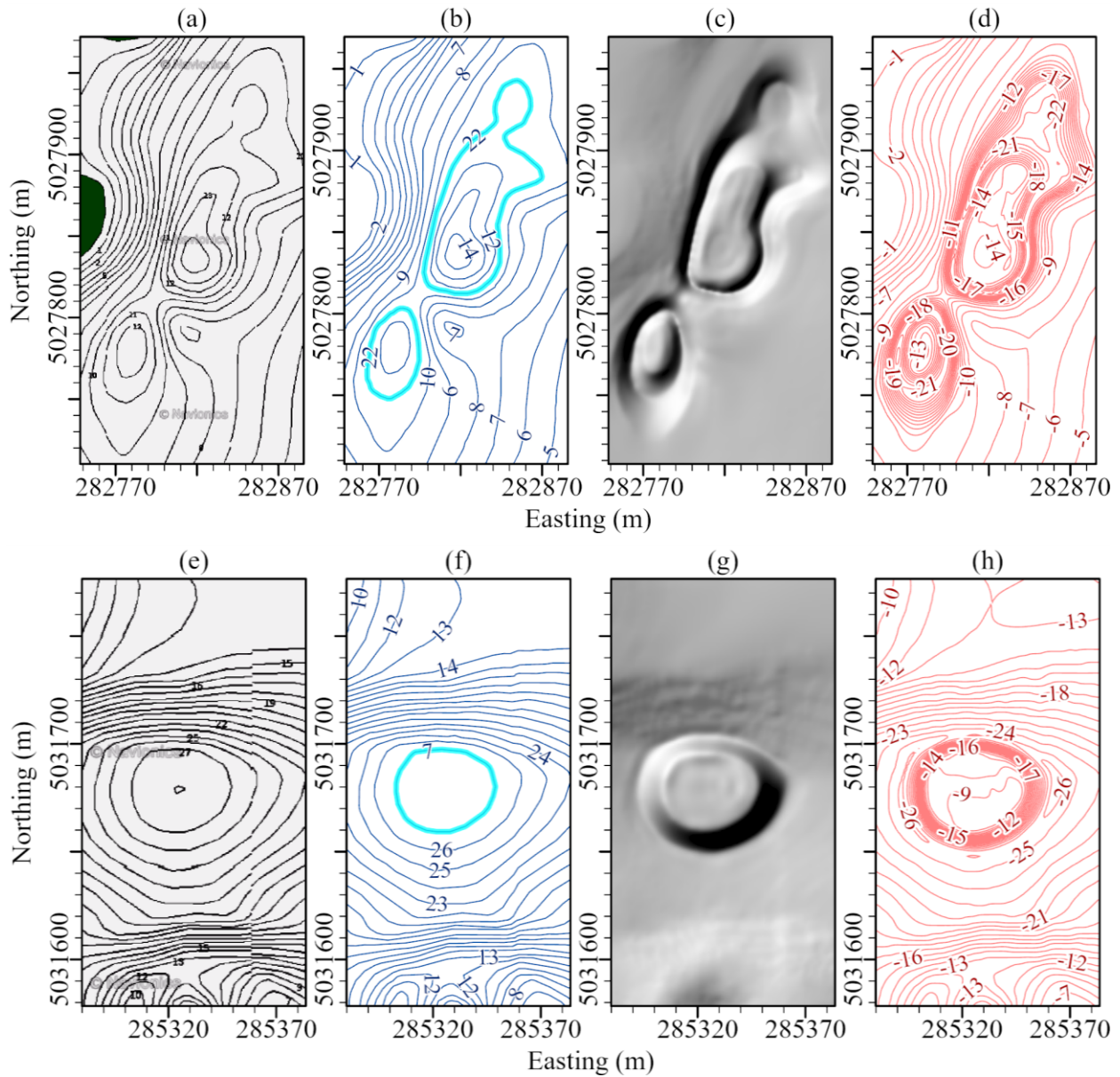


Figure-15: Incorrect depth value registered while (b)(f) digitizing contours from (a)(e) bathymetry chart; mutating the subsequent (c)(g) interpolated raster and (d)(h) interpolated vector features

5.1.3 Deviation of filtered DEM from original DEM

As discussed in section 4.3, the primary purpose of applying the slope-based filter to LiDAR T-DEM is to remove the artefacts and not affect the rest of the T-DEM. This is validated by generating a deviation raster using the following equation for denoting percentage change in raster elevations:

$$\Delta Z = \left| \frac{(Z_f - Z_r)}{Z_f} \right| \times 100 \quad \text{Eq. 4}$$

where ΔZ is the deviation of cell elevations in per cent; Z_f is the cell elevations from filtered T-DEM; Z_r is the cell elevations from the raw LiDAR T-DEM.

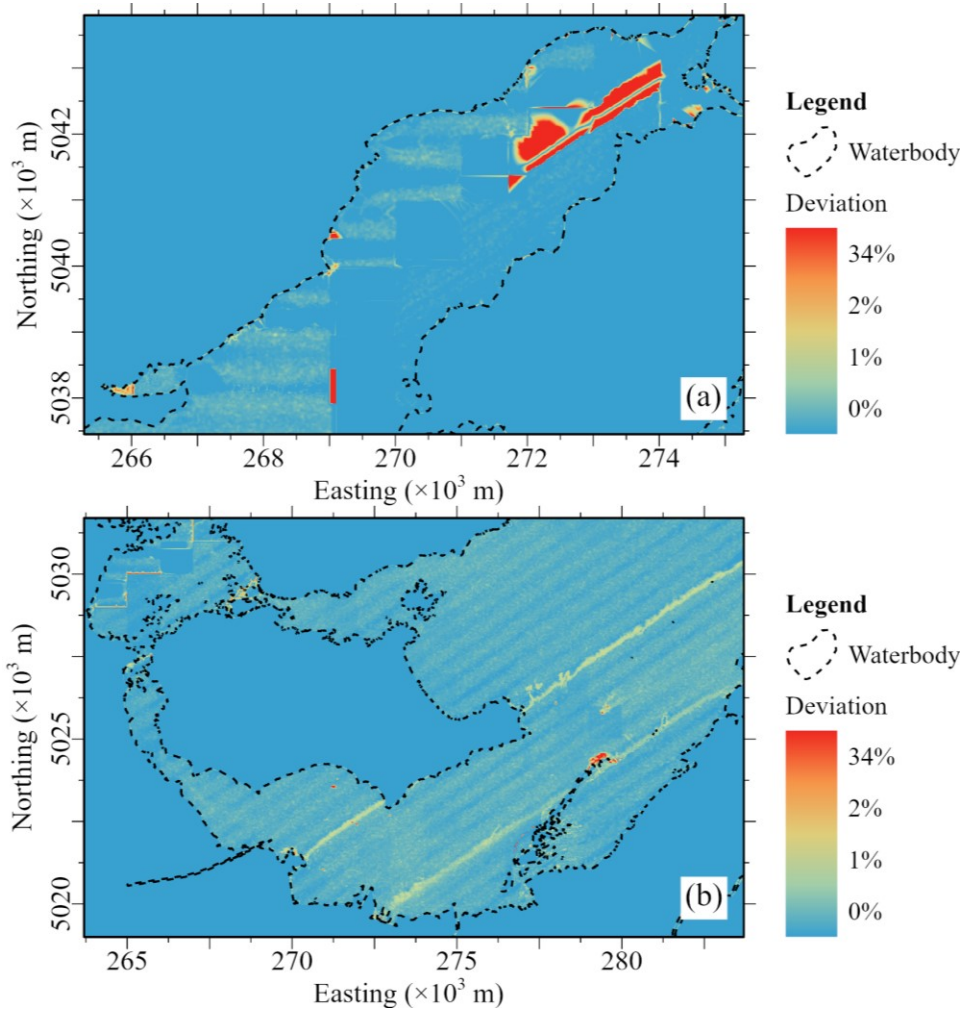


Figure-16: Raster displaying the percentage by which the filtered T-DEM deviates from the raw LiDAR T-DEM

Eq. 4 is implemented in ArcGIS on a cell-by-cell basis using the *Raster Calculator* tool to generate a deviation raster. As shown in Figure-16, the overbank region of the AOI registered no change, whereas the waterbody area experienced an overall deviation up to about 2 per cent, except few areas where the removal of artefacts resulted in significant deviations. The map also revealed the footprints of the airborne LiDAR survey. It is apparent that each survey flight passing over the water body area captured different WSE to some extent. The difference in WSEs between survey grids resulted in relatively higher slopes at grid intersections (Figure-9b) and subsequently got excluded during the slope-based filtering process. This filtered topwater surface becomes critical because the bathymetric information is numerically associated with it, and any surface anomalies present in either B-DEM or T-DEM will eventually be reflected in TB-DEM as well.

5.2 External Validation

5.2.1 Comparing B-DEM and NONNA DEMs

A direct comparison between B-DEM, NONNA-10 and NONNA-100 revealed noteworthy differences across few parameters, summarized in Table-3. The coverage of NONNA-10 is noticeably less, about 17 per cent of AOI, compared to that of B-DEM (100 per cent) and NONNA-100 (87 per cent). The lower resolution of NONNA DEMs further depreciates the quality and quantity of the bathymetric information (Figure-17). All three DEMs have similar minimum depth values, but they are dissimilar in comprehending the maximum depth values. Unlike B-DEM, the NONNA DEMs include positive elevations (land features), making them difficult to integrate statistically with any topographic DEM.

Table 3: Statistical summary of the bathymetry rasters

	B-DEM	NONNA-10	NONNA-100
Cell size (m)	1	10	100
Cell count	317889782	596115	31409
Coverage (km ²)	317.89	52.66	277.45
Minimum value (m)	-47.66	-48.46	-49.99

continued on next page

	B-DEM	NONNA-10	NONNA-100
Maximum value (m)	0.00	1.83	1.70
Range of values (m)	47.66	50.29	51.69
Mean value (m)	-4.09	-5.54	-3.25
Standard deviation (m)	4.07	4.54	3.70

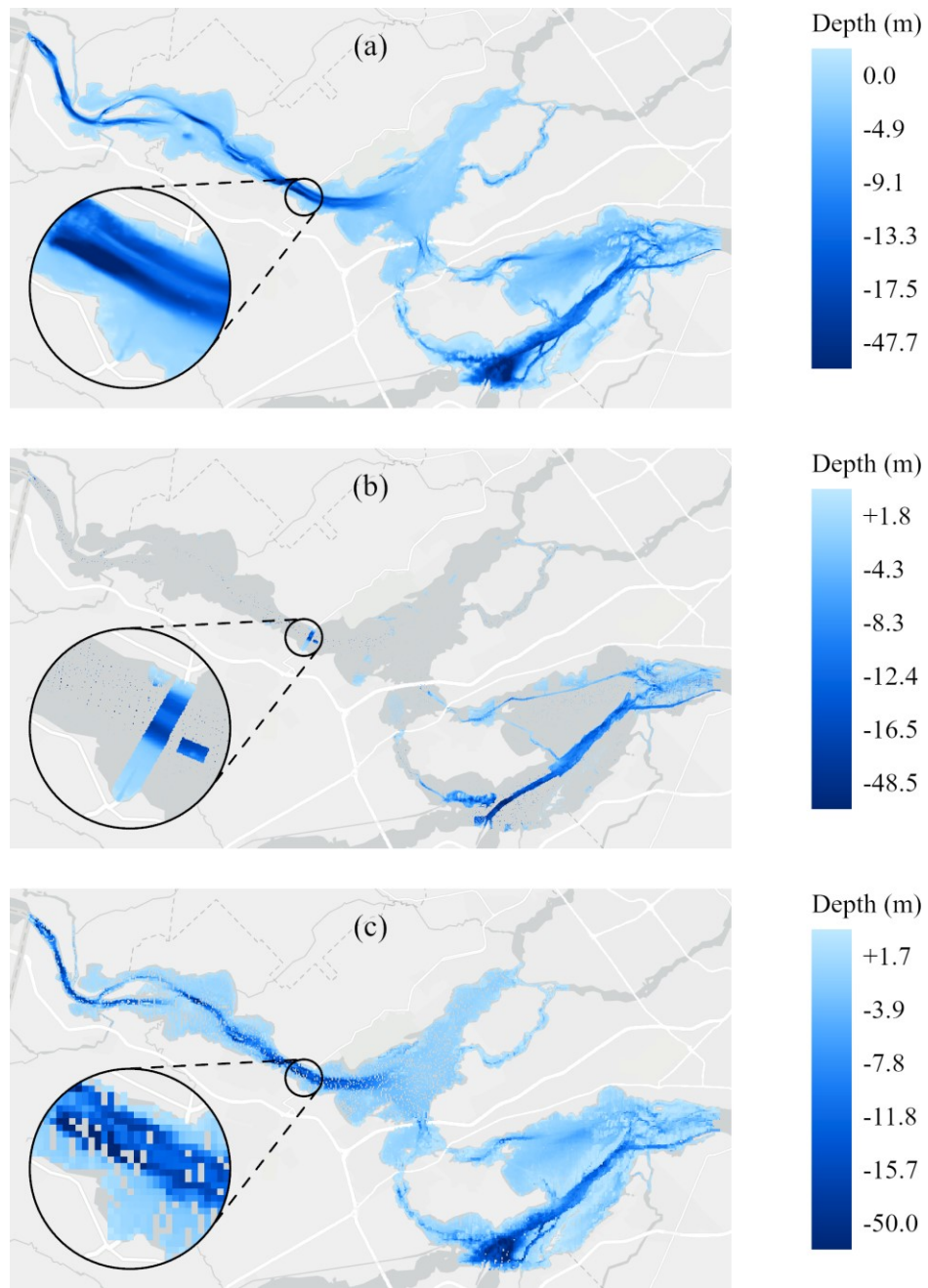


Figure-17: Comparing the coverage and data continuity of bathymetry rasters: (a) B-DEM 1m (b) NONNA-10m (c) NONNA-100m

5.2.2 Statistical validation of B-DEM using sample points

Due to the difference in coverage, a one-to-one statistical comparison between B-DEM and NONNA DEMs would not be insightful. Therefore, a sample containing point elevations from all three bathymetry rasters is generated using *Raster To Point* and *Extract To Point* tools sequentially in the ArcGIS environment. In order to cover all representative point elevations, the sample point dataset was created by converting raster cells from NONNA-10 DEM, which has the least AOI coverage among the three DEMs. A larger sample size rules out the possibility of occurring extreme sample means. Therefore, the output sample includes 584,925 points and covers almost the entire elevation range from each bathymetry raster. The same can be confirmed from minimum and maximum elevation values from bathymetry rasters and sample points (Table-3 and Table-4).

Table 4: Descriptive statistics of test sample points

	B-DEM	NONNA10	NONNA100
Mean value (m)	-6.3339	-5.6087	-4.3251
Standard error (m)	0.0064	0.0059	0.0055
Median value (m)	-5.1510	-4.3060	-2.9040
Mode value (m)	0.0000	-2.1336	0.0000
Standard deviation (m)	4.8795	4.5366	4.2164
Sample variance (m)	23.8095	20.5808	17.7776
Kurtosis	0.5831	1.0346	1.2222
Skewness	-0.9228	-1.0821	-1.2319
Range of values (m)	47.0393	50.2920	51.6892
Minimum value (m)	-47.0393	-48.4632	-49.9872
Maximum value (m)	0.0000	1.8288	1.7020
Sum of values (m)	-3704843.48	-3280649.98	-2529855.79
Count	584925	584925	584925
Confidence level (95.0%)	0.01250	0.01163	0.01081

Table 5: Correlation matrix

	B-DEM	NONNA-10	NONNA-100
B-DEM	1		
NONNA-10	0.968201	1	
NONNA-100	0.92115	0.923876	1

The sample data analysis highlighted a noticeable elevation difference at several point locations. A meaningful way is to filter the positive point elevations from NONNA-10 and compare their B-DEM elevations, as shown in Figure-18. The elevation difference visible in the bar graph points towards the detail that NONNA-10 DEM (prepared using airborne LiDAR survey) did not capture the submerged water depth as accurately as SoNAR-based B-DEM did. The sample point ID #4450, located reasonably within the water body area, is registered as a land feature in NONNA-10 DEM compared to a submerged point in B-DEM having an elevation of -8.26m.

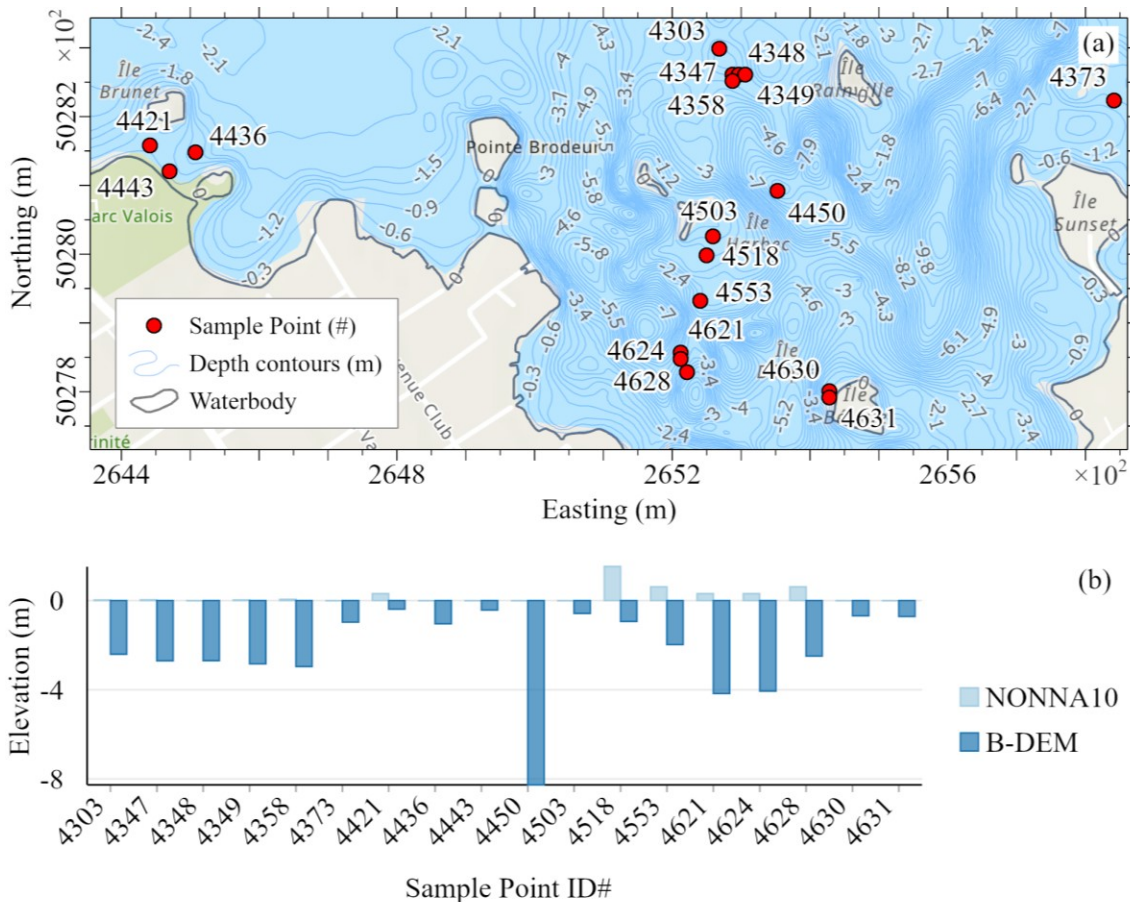


Figure-18: Comparison of sample point elevations from NONNA-10 and B-DEM

The histograms with point elevations from all three bathymetry rasters are quite similar and show a left-skewed (negative) distribution. The standard deviation of point elevations is nearly matching for B-DEM (4.88m), NONNA-10 (4.54m) and NONNA-100 (4.22m), but the dispersion over the mean is slightly wider in the case of B-DEM as shown

in Figure-19. The difference in the mean is possibly attributed to the inclusion of positive land elevations in NONNA-10 and NONNA-100. Figure-19a shows the many distributions of points near 0m elevation because the raster interpolation was constrained to a maximum elevation value of 0m. This is important for accurate superpositioning of T-DEM on B-DEM because if B-DEM has positive land elevation, it would certainly alter the upland topography undesirably.

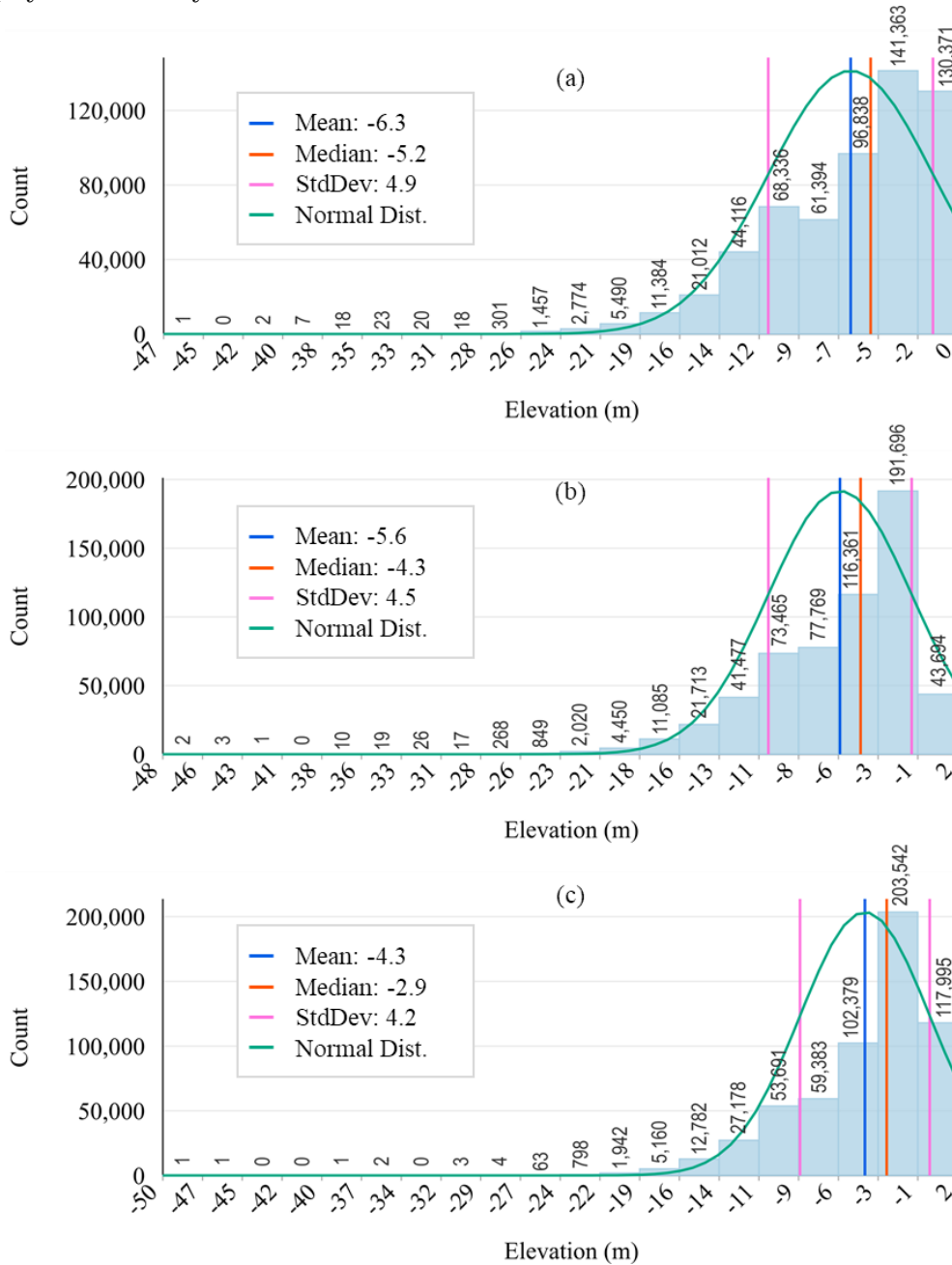


Figure-19: Histograms showing the distribution of sample points in (a) B-DEM, (b) NONNA-10 DEM and (c) NONNA-100 DEM

The scatter plot of sample point elevations between B-DEM and NONNA DEMs show large positive linear associations (Figure-20). The correlation coefficient of $r=0.968201$ between B-DEM and NONNA-10 indicates a strong relatedness of the sample point elevations. A similar relationship is observed between B-DEM and NONNA-100 (with $r=0.92115$); however, about 6.58 per cent of total sample points have positive elevations, which do not relate to B-DEM (Figure-20b). Nearly all of these points are located on the periphery of the AOI, adjacent to the bank lines, and aggregates positive elevation values of neighbouring land features due to a larger cell size of $100\text{-m} \times 100\text{-m}$.

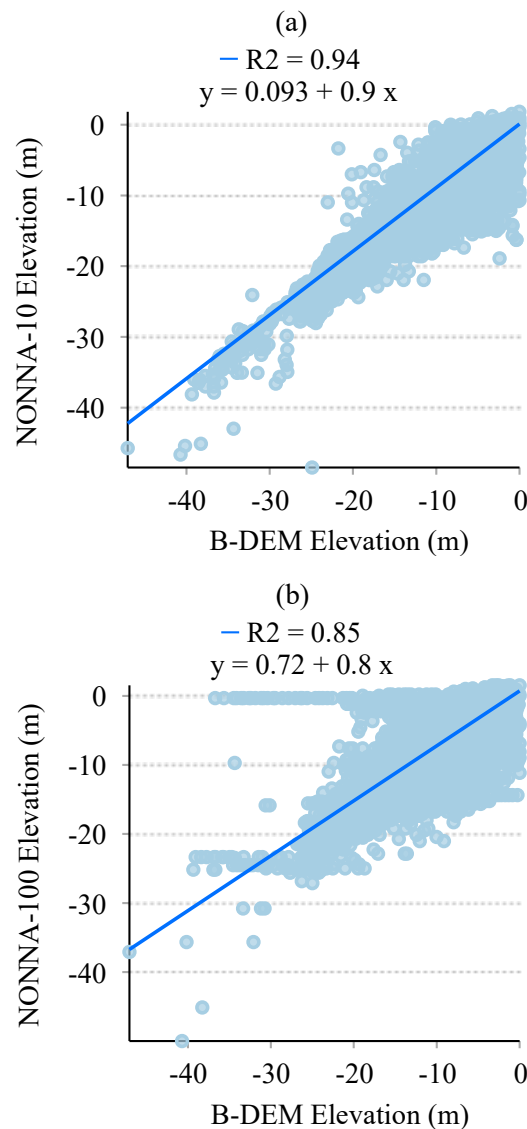


Figure-20: Scatter plot of sample point elevations showing the relationship between (a) B-DEM and NONNA-10; (b) B-DEM and NONNA-100

Another essential criterion in DEM quality assessment is calculating the root mean square error (RMSE) between the derived DEM and the reference DEM.

$$RMSE_Z = \sqrt{\frac{1}{n} \sum_{i=1}^n (Z_{di} - Z_{ci})^2} \quad \text{Eq. 5}$$

where, Z_{di} is B-DEM elevation value of an i^{th} point in the sample dataset; Z_{ci} is NONNA-10 and NONNA-100 elevation values of an i^{th} point in the sample dataset; and n is the number of sample points being checked.

The vertical accuracy in RMSE between B-DEM and NONNA-10 at native resolution is 1.4323m and between B-DEM and NONNA-100 is 2.7784m. DEMs having different resolutions are often resampled to an equal cell size before comparison, generally from higher to lower resolution. B-DEM was therefore resampled from 1m to 10m and 100m resolutions to match with that of NONNA-10 and NONNA-100, respectively. After resampling, the RMSE values are nearly identical as 1.4343m between B-DEM(10m) and NONNA-10 and 2.8692m between B-DEM(100m) and NONNA-100. The RMSE values can be considered low to medium compared to the range of elevation values in B-DEM. The lower RMSE does not necessarily mean higher accuracy of B-DEM, but it indicates that the elevation values are not far off from reference DEMs, i.e. NONNA-10 and NONNA-100. The reference datasets are certainly not of higher resolution than the B-DEM and thus not ideal for comparison. The study, therefore, requires ground control points (GCPs) for better assessing the vertical accuracy of the B-DEM.

Chapter 6:

Conclusion and Discussion

6.1 Key findings

A seamless topobathymetry DEM is generated using publicly available LiDAR-derived topography and crowdsourced bathymetry data. At first, the crowdsourced bathymetry, which is usually not available in ready-to-use digital data format, is collected, pre-processed, georeferenced, and digitized to generate an inverted DEM representing the channel bathymetry as depth measurements. Next, the LiDAR DEM is superpositioned onto the bathymetry DEM such that only the channel depth measurements are numerically added to the LiDAR elevations without affecting the upland topography. As a result, an integrated DEM is generated, which describes the channel and floodplain geometry accurately and entirely. The study also proposes a novel and simple superposition-based approach for combining topography and bathymetry datasets along with spatial and temporal prerequisites. As input datasets, it requires published LiDAR DEM and processed bathymetry information (either in digital data format or paper chart). The proposed method can be applied to other areas if both the input datasets are sufficiently available. It does not require ground measurements or data collection, provided that the input datasets have sufficient ground control points for accurate georeferencing.

Key findings from the study are as follows:

- 1) There is substantial potential for crowdsourced bathymetry in developing seamless terrain models for hydraulic modelling purposes.
- 2) The input LiDAR T-DEM is unchanged except waterbody area. Therefore, it can be stated that the vertical accuracy of LiDAR T-DEM remains intact, except in the waterbody area where the vertical accuracy is attributed to that of B-DEM.
- 3) The B-DEM elevations show a strong correlation with that of NONNA-10 and

NONNA-100 datasets. The vertical difference between B-DEM and NONNA-10 is 1.43m for RMSE, while 2.78m between B-DEM and NONNA-100.

- 4) The integrated TB-DEM is superior to source LiDAR T-DEM and crowdsourced B-DEM regarding coverage and continuity of elevation information.
- 5) The riverbank line is a critical element in deciding the extent to which the bathymetric information will be interpolated. The interpolation extent directly impacts the accuracy of superpositioning the disparate elevation datasets.
- 6) The DTM filter (slope-based) is not an exhaustive DEM correction method as it did not filter out all types of artefacts.
- 7) Temporal prerequisite must be adhered to for an accurate superpositioning of T-DEM onto B-DEM.
- 8) The proposed approach can be automated entirely once the input data quality and quantity is attained to a certain extent.

The seamless topobathymetry DEM is created as a single-band georeferenced raster file (*.tif*) with a cell size of 1-m \times 1-m. The *.tif* file is recognized by most popular GIS programs but may not be readable by some hydraulic and habitat modelling programs. Since TB-DEM was first produced using ArcGIS - a licensed proprietary software; the output TB-DEM is also exported separately in an American Standard Code for Information Interchange (ASCII) text file format (*.txt*), which can be imported and used in other non-proprietary programs as well. Due to the enormous size of the output file, TB-DEM is divided into fifteen smaller grids, as shown in Appendix-A. An ASCII-format raster (*.txt*) file begin with header information that defines raster properties such as the number of rows and columns, the cell size, and the coordinates of the origin of the raster. The header information is followed by cell value information, in this case, elevation in meter, in space-delimited row order. The spatial location of the raster is specified by the location of the lower-left corner of the lower-left cell (Appendix-B, sample file: *tbDEM_08.txt*). An ASCII-format raster is often accompanied by a *.prj* file that describes the spatial reference properties and the coordinate system used by the ASCII-format raster (Appendix-B, sample file: *TBDEM.prj*).

6.2 Applications of Topobathymetry DEM

The high-resolution TB-DEM developed in this study has many applications in the domain of hydraulic and ecohydraulic modelling. It can be used as critical input data in studies related to flood modelling. The elevation tolerance requirements vary based on the intended use of a DEM. In general floodplain mapping and flood control studies, the required elevation tolerance can be 0.2 - 2 ft with a contour interval ranging from 2 - 5 ft; for flood insurance studies, the elevation tolerance is 0.5 ft with a contour interval of 4 ft; and for actual siting of structures, the vertical tolerances of 0.05 - 1 ft with contour intervals of 0.5 - 1 ft are typical (Dyhouse et al., 2003). The TB-DEM is generated using the bathymetry available at 1-ft contour interval and, therefore, it can be used appropriately for floodplain mapping, flood insurance studies and site feasibility assessment of hydraulic structures such as storage reservoirs.

The other important application is to use TB-DEM as input data for instream habitat evaluation studies. The change in fish habitat with stream flows is commonly predicted using instream habitat models. They comprise a hydrodynamic model to predict water depth and flow velocity; and a biological model to predict habitat quality for fish using water depth, flow velocity and substrate composition (Guay et al., 2000). A high-resolution river bathymetry data allows 2D hydrodynamic models to accurately estimate discharge value, which is vital in aquatic habitat modelling to characterize the habitat quality distribution (Benjankar et al., 2018).

A two-dimensional hydraulic and habitat model, such as River2D, is used to predict depth and velocity at given streamflow values and combine them with the substrate to predict habitat indices like weighted usable area (Gard, 2009). In 2D models, the accuracy of topographic input data significantly affects the accuracy of depth and velocity prediction, which is particularly important in braided rivers (Frank et al., 2007; Jowett et al., 2012). Crowder and Diplas (2000) demonstrated that the presence or absence of bathymetry data in a 2D model could significantly influence predicted flow patterns important to aquatic habitat. While bathymetry data generated from field surveys (cross-

sectional data) tend to lose morphological details due to the smoothing of riverbed topography between cross-sections, a 2D bathymetry data would allow the hydro-morphological model to accurately define the position of erosional-depositional areas and determine morphological tendencies necessary for instream habitat evaluation (Frank et al., 2007). Gard (2009) found specific errors in habitat predictions using 2D model due to: (a) inadequate detail in mapping substrate distribution, (b) insufficient data to correctly map the bed topography, and (c) effects of the upstream bed topography not being included in the model. The high-resolution (1m) TB-DEM generated in this study provide a complete description of the riverbed and floodplain topography and can conceivably reduce, if not remove, the errors due to the abovementioned reasons. Iampietro et al. (2005) demonstrated and validated a similar use case of a high-resolution (2m) multibeam bathymetry DEM in a habitat suitability model for eight rockfish species, capable of capturing an average of approximately 80% of all eight rockfish species on the seabed.

TB-DEM can also be used in the planning of mitigation and restoration measures for fish habitat enhancement. A similar study has demonstrated that the 2D modelling approach could successfully simulate the inundated areas and flow patterns that are important for planning mitigation and restoration measures in rivers (Adeva-Bustos et al., 2019).

Shoreline erosion has various and adverse consequences on both the riverine and marine environments. Thoma et al. (2005) used annually collected airborne LiDAR-derived DEMs (1m spatial resolution) to determine volume change over time by differentiating the DEMs and illustrated that laser scanning could be used to estimate the contribution of eroded bank materials to the total sediment load. The TB-DEM generated in this study uses a LiDAR DEM having a similar spatial resolution, along with the regularly updated crowdsourced bathymetry, which could help investigate the spatial and temporal variations of riverbank erosion and estimate the rate of sediment production.

Hydraulic models are also used to identify and evaluate potential locations for water intake or effluent disposal along the riverbank. Ajiwibowo (2018) carried out numerical

modelling to develop a sedimentation analysis and further deduce the best locations of the water effluent outlet. The study employed a boat-based single beam echosounder survey to map bathymetry with a sounding gap of 50m. Because the study was focused on a regional scale, the bathymetric information at a minimum scale of 1:200,000 was sufficient for study objectives. It can be inferred that a high-resolution Topo-bathymetric DEM would certainly be appropriate for such site selection studies focused at a local level.

6.3 Examples from around the world

With the advancement in LiDAR and Multibeam SoNAR-based survey methods, high-resolution topography and bathymetry datasets are increasingly becoming available. Although disparate multi-temporal data sources have been extensively used in hydraulic, hydromorphological and ecohydraulic modelling applications, researchers have started exploring advanced sensing technologies and new methods for integrating such disparate data sources. As a result, several studies focused on developing seamless topo-bathymetric DEM have been published in recent years. Chowdhury et al. (2017) generated topo-bathymetry DEM for Lower Athabasca River Watershed in Alberta, Canada, using Geoswath bathymetry (5-10 m spatial resolution), point cloud LiDAR data and river cross-section data. U.S. Geological Survey has developed Coastal National Elevation Database (CoNED) by developing coastal topobathymetric elevation models from multiple topographic, intertidal topobathymetric and offshore bathymetric data sources. The CoNED now includes integrated topobathymetric elevation models for Mobile Bay, the northern Gulf of Mexico, San Francisco Bay, the Hurricane Sandy region, and southern California (Danielson et al., 2016). Most recently, the U.S. Army Corps of Engineers has created a seamless DEM for the Mississippi River in the State of Louisiana (Arnold, 2020). These seamless DEMs are created at the spatial resolution of 1 m, 2 m, 5 m, and 10 m to support hydrologic modelling studies. Wilson and Power (2018) created three seamless bathymetry and coastal topography datasets for New South Wales, Australia, with an intention to research tsunami modelling. The input DEMs had varying data resolution and densities, which indicates the output DEM resolution between 1-5 m. The

abovementioned DEMs have been developed based on extensively surveyed raw input data that are essentially disparate by nature and lack temporal dimension. On the contrary, the TB-DEM generated in this study relies on crowdsourced bathymetry data that is regularly updated as the new depth readings are gathered and transmitted by the ‘crowd’, thereby capturing spatial and temporal changes in the bathymetry.

6.4 Future studies

The future version of the study will include the collection of ground control points and subsequent validation of the TB-DEM elevations in the AOI. The validity and applicability of the superposition-based approach presented in this study shall further be investigated by developing TB-DEMs for other areas and comparing their accuracy in RMSE with available higher resolution reference data. The integrated TB-DEM created in this study is in the format that is readable and acceptable by popular hydraulic modelling programs. Therefore, the study encourages researchers and hydraulic modellers to test the applicability of TB-DEM in their respective studies and verify the accuracy of modelling results.

Bibliography

- Adeva-Bustos, A., Alfredsen, K., Fjeldstad, H.P. and Ottosson, K., (2019). Ecohydraulic modelling to support fish habitat restoration measures. *Sustainability*, 11(5), p.1500.
- Ajiwibowo, H., (2018). Numerical modeling for the selection of effluent outlet location. *International Journal of Geomate*, 14(45), pp.192-201.
- Arnold, D.E., (2020). Seamless Digital Elevation Model (DEM) creation for the Mississippi River in Louisiana to support hydrologic modeling. ARMY CORPS OF ENGINEERS VICKSBURG MS VICKSBURG.
- Bailly, J., Le Coarer, Y., Languille, P., Stigermark, C., & Allouis, T. (2010). Geostatistical estimations of bathymetric LiDAR errors on rivers. *Earth Surface Processes and Landforms*, 35(10), 1199-1210. doi:10.1002/esp.1991
- Benjankar, R., Tonina, D., McKean, J.A., Sohrabi, M.M., Chen, Q. and Vidergar, D., (2019). An ecohydraulics virtual watershed: Integrating physical and biological variables to quantify aquatic habitat quality. *Ecohydrology*, 12(2), p.e2062.
- Benke, A. C., & Cushing, C. E. (2005). *Rivers of north america*. Amsterdam: Elsevier/ Academic Press. Retrieved from <https://concordiauniversity.on.worldcat.org/oclc/59003378>
- Berghuijs, W. R., Aalbers, E. E., Larsen, J. R., Trancoso, R., & Woods, R. A. (2017). Recent changes in extreme floods across multiple continents. *Environmental Research Letters*, 12(11), 114035.
- Berghuijs, W.R., Woods, R.A., Hutton, C.J. and Sivapalan, M. (2016). Dominant flood generating mechanisms across the United States. *Geophysical Research Letters*, 43(9), pp.4382-4390.
- Bhuyian, M. N. M., Kalyanapu, A. J., & Nardi, F. (2015). Approach to digital elevation model correction by improving channel conveyance. *Journal of Hydrologic Engineering*, 20(5) doi:10.1061/(ASCE)HE.1943-5584.0001020
- Bures, L., Roub, R., Sychova, P., Gdulova, K., & Doubalova, J. (2019). Comparison of bathymetric data sources used in hydraulic modelling of floods. *Journal of Flood*

Risk Management, 12(S1) doi:10.1111/jfr3.12495

- Bures, L., Sychova, P., Maca, P., Roub, R., & Marval, S. (2019). River bathymetry model based on floodplain topography. *Water*, 11(6), 1287. doi:10.3390/w11061287
- Callow, J. N., Van Niel, K. P., & Boggs, G. S. (2007). How does modifying a DEM to reflect known hydrology affect subsequent terrain analysis? *Journal of Hydrology*, 332(1-2), 30-39. doi:10.1016/j.jhydrol.2006.06.020
- Chen, W., Nover, D., He, B., Yuan, H., Ding, K., Yang, J., & Chen, S. (2018). Analyzing inundation extent in small reservoirs: A combined use of topography, bathymetry and a 3D dam model. *Measurement*, 118, 202-213. doi:10.1016/j.measurement.2018.01.042
- Chowdhury, E.H., Hassan, Q.K., Achari, G. and Gupta, A., (2017). Use of bathymetric and LiDAR data in generating digital elevation model over the Lower Athabasca River Watershed in Alberta, Canada. *Water*, 9(1), p.19.
- CHS. (2020). NONNA data portal. Retrieved from <https://data.chs-shc.ca/login>
- Conner, J. T., & Tonina, D. (2014). Effect of cross-section interpolated bathymetry on 2D hydrodynamic model results in a large river. *Earth Surface Processes and Landforms*, 39(4), 463-475. doi:10.1002/esp.3458
- Cook, A., & Merwade, V. (2009). Effect of topographic data, geometric configuration and modeling approach on flood inundation mapping. *Journal of Hydrology*, 377(1), 131-142. doi:10.1016/j.jhydrol.2009.08.015
- Corum, Z. P., Ball, T. D., & Hubbard, M. J. (2015). Synthetic bathymetry method development, validation and application to five pacific northwest rivers. Retrieved from <https://acwi.gov/sos/pubs/3rdJFIC/Contents/5D-Corum.pdf>
- Costa, B. M., Battista, T. A., & Pittman, S. J. (2009). Comparative evaluation of airborne LiDAR and ship-based multibeam SoNAR bathymetry and intensity for mapping coral reef ecosystems. *Remote Sensing of Environment*, 113(5), 1082-1100. doi:10.1016/j.rse.2009.01.015
- Crowder, D.W. and Diplas, P., (2000). Using two-dimensional hydrodynamic models at scales of ecological importance. *Journal of hydrology*, 230(3-4), pp.172-191.

- Danielson, J. J., Poppenga, S. K., Brock, J. C., Evans, G. A., Tyler, D. J., Gesch, D. B., . . . Barras, J. A. (2016). Topobathymetric elevation model development using a new methodology: Coastal national elevation database. *Journal of Coastal Research*, (76), 75-89.
- Dey, S. (2016). *Role of river bathymetry in hydraulic modeling of river channels*
Retrieved from https://docs.lib.purdue.edu/open_access_theses/940
- Do, H. X., Mei, Y. and Gronewold, A. D. (2020). To what extent are changes in flood magnitude related to changes in precipitation extremes?. *Geophysical Research Letters*, 47(18), p.e2020GL088684.
- DFO-Science CHS Strategic Directions and Quality Policy 2018/28, (2018). Retrieved from <https://www.charts.gc.ca/help-aide/about-apropos/strategic-strategiques-eng.html>
- Dyhouse, G., Hatchett, J. and Benn, J., (2003). *Floodplain modeling using HEC-RAS*. Haestad press.
- ESRI. (2018). Understanding raster georeferencing. Retrieved from <https://www.esri.com/about/newsroom/wp-content/uploads/2018/07/Understanding-Raster-Georeferencing.pdf>
- Falcão, A. P., Matias, M. P., Pestana, R., Gonçalves, A. B., & Heleno, S. (2016). Methodology to combine topography and bathymetry data sets for hydrodynamic simulations: Case of tagus river. *Journal of Surveying Engineering*, 142(4), 05016005. doi:10.1061/(ASCE)SU.1943-5428.0000192
- Farina, G., Alvisi, S., Franchini, M., Corato, G., & Moramarco, T. (2015). Estimation of bathymetry (and discharge) in natural river cross-sections by using an entropy approach. *Journal of Hydrology*, 527, 20-29. doi:10.1016/j.jhydrol.2015.04.037
- Flanagin, M., Grenotton, A., Ratcliff, J., Shaw, K. B., Sample, J., & Abdelguerfi, M. (2008). Hydraulic splines: A hybrid approach to modeling river channel geometries. *Computing in Science & Engineering.*, 9(5), 4-15. Retrieved from <https://concordiauniversity.on.worldcat.org/oclc/8508259726>
- Flener, C., Lotsari, E., Alho, P., & Käyhkö, J. (2012). Comparison of empirical and theoretical remote sensing based bathymetry models in river environments. *River Research and Applications*, 28(1), 118-133. doi:10.1002/rra.1441

- Frank, E., Montoya, M. and Fattorelli, S., (2007). Effects of topographic data resolution and spatial model resolution on a bi-dimensional hydro-morphological model. *WIT Transactions on Ecology and the Environment*, 104, pp.325-334.
- Fregoso, T. A., Wang, R., Ateljevich, E., & Jaffe, B. E. (2017). A new seamless, high-resolution digital elevation model of the san francisco bay-delta estuary, california. Retrieved from <https://doi.org/10.3133/ofr20171067>
- Gard, M., (2009). Comparison of spawning habitat predictions of PHABSIM and River2D models. *International Journal of River Basin Management*, 7(1), pp.55-71.
- Gesch, D. B., Brock, J. C., Parrish, C. E., Rogers, J. N., & Wright, C. W. (2016). Introduction: Special issue on advances in topobathymetric mapping, models, and applications. *Journal of Coastal Research*, 76(sp1), 1-3. doi:10.2112/SI76-001
- Gouvernement du Québec. (2021). The st. lawrence. Retrieved from <https://www.planstlaurent.qc.ca/en/st-lawrence-river>
- Guay, J.C., Boisclair, D., Rioux, D., Leclerc, M., Lapointe, M. and Legendre, P., (2000). Development and validation of numerical habitat models for juveniles of Atlantic salmon (*Salmo salar*). *Canadian Journal of Fisheries and Aquatic Sciences*, 57(10), pp.2065-2075.
- Henstra, D., & Thistlethwaite, J. (2018). Flood risk mapping in canada: Moving forward on a national priority.
- Hutchinson, M. F. (2011). ANUDEM version 5.3, user guide. *Canberra: Fenner School of Environment and Society, Australian National University*,
- Iampietro, P.J., Kvitek, R.G. and Morris, E., (2005). Recent advances in automated genus-specific marine habitat mapping enabled by high-resolution multibeam bathymetry. *Marine Technology Society Journal*, 39(3), pp.83-93.
- IPCC, 2021: Summary for Policymakers. In: *Climate Change 2021: The Physical Science Basis. Contribution of Working Group I to the Sixth Assessment Report of the Intergovernmental Panel on Climate Change* [MassonDelmotte, V., P. Zhai, A. Pirani, S. L. Connors, C. Péan, S. Berger, N. Caud, Y. Chen, L. Goldfarb, M. I. Gomis, M. Huang, K. Leitzell, E. Lonnoy, J. B. R. Matthews, T. K. Maycock, T. Waterfield, O. Yelekçi, R. Yu and B. Zhou]. *Cambridge University Press*. In Press.

- Journault, M., Maltais, L., & Sanfacon, R. (2012). High precision hydrography in Canada, the St. Lawrence river channel, HD bathymetry, production, distribution and updating.
- Jowett, I.G. and Duncan, M.J., (2012). Effectiveness of 1D and 2D hydraulic models for instream habitat analysis in a braided river. *Ecological Engineering*, 48, pp.92-100.
- Kinzel, P. J., Legleiter, C. J., & Nelson, J. M. (2013). Mapping river bathymetry with a small footprint green LiDAR: Applications and challenges. *JAWRA Journal of the American Water Resources Association*, 49(1), 183-204. doi:10.1111/jawr.12008
- Kreienkamp, F. (2021). Rapid attribution of heavy rainfall events leading to the severe flooding in Western Europe during July 2021. World Weather Attribution. Retrieved from <http://repo.floodalliance.net/jspui/handle/44111/4335>
- Lai, R., Wang, M., Yang, M., & Zhang, C. (2018). Method based on the Laplace equations to reconstruct the river terrain for two-dimensional hydrodynamic numerical modeling. *Computers and Geosciences*, 111, 26-38. doi:10.1016/j.cageo.2017.10.006
- Laks, I., Sojka, M., Walczak, Z., & Wróżyński, R. (2017). Possibilities of using low quality digital elevation models of floodplains in hydraulic numerical models. *Water*, 9(4) doi:10.3390/w9040283
- Legleiter, C. J. (2021). The optical river bathymetry toolkit. *River Research and Applications*, 37(4), 555-568. doi:10.1002/rra.3773
- Li, Z., Zhu, C., & Gold, C. (2004). *Digital terrain modeling: Principles and methodology* CRC press.
- Loftis, J. D., Wang, H. V., DeYoung, R. J., & Ball, W. B. (2016). Using lidar elevation data to develop a topobathymetric digital elevation model for sub-grid inundation modeling at Langley Research Center. *Journal of Coastal Research*, 76(sp1), 134-148. doi:10.2112/SI76-012
- Loftis, J. D., Wang, H. V., DeYoung, R. J., & Ball, W. B. (2016). Using lidar elevation data to develop a topobathymetric digital elevation model for sub-grid inundation modeling at Langley Research Center. *Journal of Coastal Research*, 76(sp1), 134-148. doi:10.2112/SI76-012

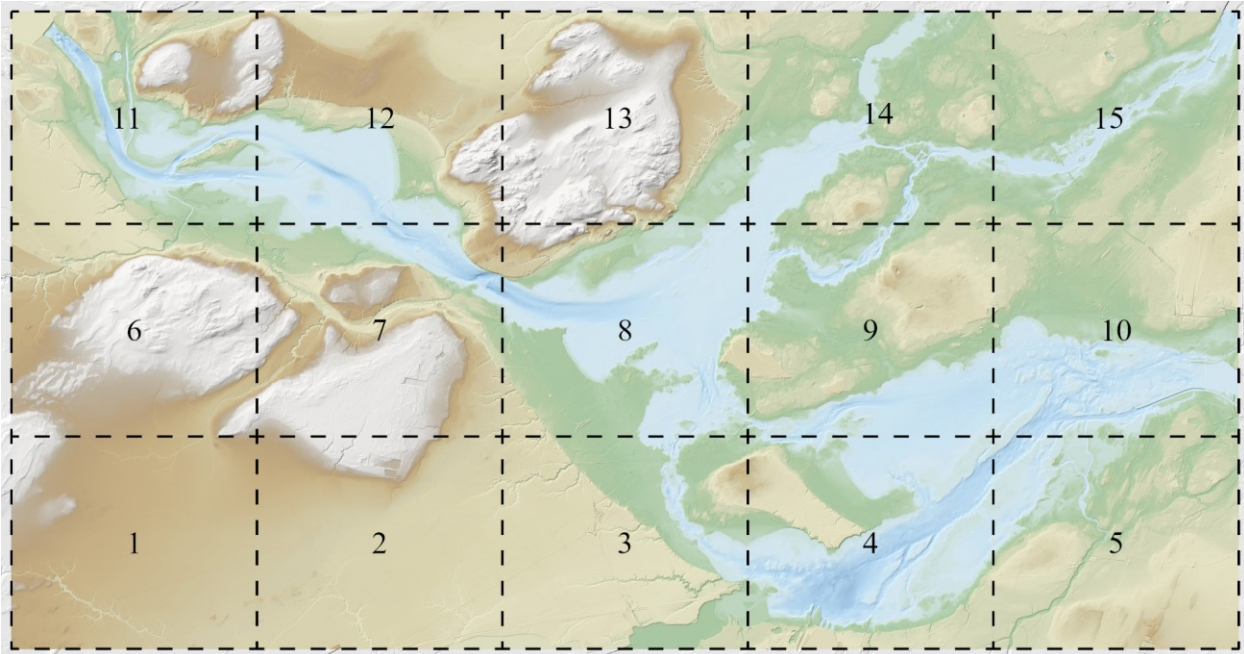
- McGrath, M. Z., Ozeren, Y., & Altinakar, M. S. (2017). Generation of 2D riverbed topography for digital elevation models using 1D cross-section data. Paper presented at the *World Environmental and Water Resources Congress 2017*, 402-415. Retrieved from <https://doi.org/10.1061/9780784480625.037>
- NOAA. (2021). What is bathymetry? Retrieved from <https://oceanservice.noaa.gov/facts/bathymetry.html>
- ORRPB. (2021). Ottawa river at carillon. Retrieved from <http://ottawariver.ca/information/historical-water-level-streamflow-summary/ottawa-river-at-carillon/>
- Ottawa Riverkeeper. (2021). FAQs on the carillon dam and the american eel. Retrieved from <https://www.ottawariverkeeper.ca/faqs-on-the-carillon-dam-and-the-american-eel/>
- Park, E., Emadzadeh, A., Alcântara, E., Yang, X., & Ho, H. L. (2020). Inferring floodplain bathymetry using inundation frequency. *Journal of Environmental Management*, 273, 111138. doi:10.1016/j.jenvman.2020.111138
- Polidori, L., & Hage, M. E. (2020). Digital elevation model quality assessment methods: A critical review. *Remote Sensing*, 12(3522) doi:10.3390/rs12213522
- Quadros, N. D., Collier, P. A., & Fraser, C. S. (2008). Integration of bathymetric and topographic LiDAR: A preliminary investigation. *The International Archives of the Photogrammetry, Remote Sensing and Spatial Information Sciences*, 36, 1299-1304.
- Seneviratne, S. I., X. Zhang, M. Adnan, W. Badi, C. Dereczynski, A. Di Luca, S. Ghosh, I. Iskandar, J. Kossin, S. Lewis, F. Otto, I. Pinto, M. Satoh, S. M. Vicente-Serrano, M. Wehner, B. Zhou, (2021). Weather and Climate Extreme Events in a Changing Climate. In: *Climate Change 2021: The Physical Science Basis. Contribution of Working Group I to the Sixth Assessment Report of the Intergovernmental Panel on Climate Change. Cambridge University Press. In Press.*
- Skinner, K. D. (2009). *Evaluation of LiDAR-acquired bathymetric and topographic data accuracy in various hydrogeomorphic settings in the lower boise river, southwestern idaho, 2007.* (). Retrieved from <https://pubs.usgs.gov/sir/2009/5260/>
- Tarekegn, T. H., Haile, A. T., Rientjes, T., Reggiani, P., & Alkema, D. (2010). Assessment of an ASTER-generated DEM for 2D hydrodynamic flood modeling. *International Journal of Applied Earth Observations and Geoinformation*, 12(6),

457-465. doi:10.1016/j.jag.2010.05.007

- Thoma, D. P., Gupta, S. C., Bauer, M. E. and Kirchoff, C. E., (2005). Airborne laser scanning for riverbank erosion assessment. *Remote sensing of Environment*, 95(4), pp.493-501.
- Vaze, J., Teng, J., & Spencer, G. (2010). Impact of DEM accuracy and resolution on topographic indices. *Environmental Modelling and Software*, 25(10), 1086-1098. doi:10.1016/j.envsoft.2010.03.014
- Vosselman, G. (2000). Slope based filtering of laser altimetry data. *International Archives of Photogrammetry and Remote Sensing*, 33(B3/2; PART 3), 935-942.
- Walczak, Z., Sojka, M., Wróżyński, R., & Laks, I. (2016). Estimation of polder retention capacity based on ASTER, SRTM and LIDAR DEMs: The case of majdany polder (west poland). *Water*, 8(6) doi:10.3390/w8060230
- Wang, R., Ateljevich, E., Fregoso, T. A., & Jaffe, B. E. (2019). A revised continuous surface elevation model for modeling. *39th annual progress report to the state water resources control board* (pp. 5-40) California Department of Water Resources, Bay-Delta Office. Retrieved from <https://pubs.er.usgs.gov/publication/70204415>
- Wilson, K. M., & Power, H. E. (2018). Seamless bathymetry and topography datasets for new south wales, australia. *Scientific Data*, 5(1) doi:10.1038/sdata.2018.115
- Yamazaki, D., Baugh, C. A., Bates, P. D., Kanae, S., Alsdorf, D. E., & Oki, T. (2012). Adjustment of a spaceborne DEM for use in floodplain hydrodynamic modeling. *Journal of Hydrology*, 436-437, 81-91. doi:10.1016/j.jhydrol.2012.02.045
- Yoon, Y., Durand, M., Merry, C. J., Clark, E. A., Andreadis, K. M., & Alsdorf, D. E. (2012). Estimating river bathymetry from data assimilation of synthetic SWOT measurements. *Journal of Hydrology*, 464-465, 363-375. doi:10.1016/j.jhydrol.2012.07.028

Appendices

Appendix A: TB-DEM grid



File Name	File Type	Size	Date Modified
TBDEM.prj	Coordinate Reference System	359 B	9/10/21, 10:38:14 PM
tbdem_01.txt	ASCII Text Document	664 MB	9/10/21, 10:38:14 PM
tbdem_02.txt	ASCII Text Document	663 MB	9/10/21, 10:18:38 PM
tbdem_03.txt	ASCII Text Document	687 MB	9/10/21, 10:16:53 PM
tbdem_04.txt	ASCII Text Document	859 MB	9/10/21, 10:39:55 PM
tbdem_05.txt	ASCII Text Document	704 MB	9/10/21, 10:36:39 PM
tbdem_06.txt	ASCII Text Document	702 MB	9/10/21, 10:33:26 PM
tbdem_07.txt	ASCII Text Document	725 MB	9/10/21, 10:30:13 PM
tbdem_08.txt	ASCII Text Document	848 MB	9/10/21, 10:26:58 PM
tbdem_09.txt	ASCII Text Document	763 MB	9/10/21, 10:23:36 PM
tbdem_10.txt	ASCII Text Document	780 MB	9/10/21, 10:35:05 PM
tbdem_11.txt	ASCII Text Document	824 MB	9/10/21, 10:31:50 PM
tbdem_12.txt	ASCII Text Document	844 MB	9/10/21, 10:28:35 PM
tbdem_13.txt	ASCII Text Document	813 MB	9/10/21, 10:25:20 PM
tbdem_14.txt	ASCII Text Document	797 MB	9/10/21, 10:22:00 PM
tbdem_15.txt	ASCII Text Document	755 MB	9/10/21, 10:20:17 PM

Appendix B: Sample of ASCII file content

tbdem_08.txt

(ASCII Text Document)

```
ncols      11666
nrows      10082
xllcorner  257389.15002737
yllcorner  5028558.9074159
cellsize   1
NODATA_value -9999
78.68999 78.66 78.71 78.63 78.58 78.56 78.61 78.56 78.62 78.6 78.55
78.56 78.68999 78.78 78.82 78.84 78.93999 78.95 79 79.03 79.03 79.09
79.11 79 79.25999 79.3 79.2 79.14 79.09 79.13 79.25999 79.24 79.23
79.28 79.29 79.5 79.61 79.65 79.67 79.73 79.8 79.78 . . . . .
```

TBDEM.prj

(Coordinate Reference System)

```
Projection  TRANSVERSE
Datum       AI_CSRS
Spheroid    GRS80
Units       METERS
Zunits      NO
Xshift      0.0
Yshift      0.0
Parameters
0.9999 /* scale factor at central meridian
-73 30 0.0 /* longitude of central meridian
  0 0 0.0 /* latitude of origin
304800.0 /* false easting (meters)
0.0 /* false northing (meters)
```